

Article

Bis-Citrullinato Copper(II) Complex: Synthesis, Crystal Structure, and Non-Covalent Interactions

Diego Ramírez-Contreras ¹, Amalia García-García ^{1,2} , Brenda L. Sánchez-Gaytán ¹,
Laura E. Serrano-de la Rosa ³ , Francisco J. Melendez ⁴ , Duane Choquesillo-Lazarte ⁵ ,
Antonio Rodríguez-Diéguez ² , María Eugenia Castro ^{1,*}  and Enrique González-Vergara ^{1,*} 

¹ Centro de Química del Instituto de Ciencias, Benemérita Universidad Autónoma de Puebla, 18 sur y Av. San Claudio, Col. San Manuel, Puebla 72570, Mexico

² Departamento de Química Inorgánica, Facultad de Ciencias, Universidad de Granada, Av. Fuentenueva S/N, 18071 Granada, Spain

³ Laboratorio Central del Instituto de Física “Luis Rivera Terrazas” (IFUAP), Benemérita Universidad Autónoma de Puebla, 18 sur y Av. San Claudio, Col. San Manuel, Puebla 72570, Mexico

⁴ Lab. de Química Teórica, Centro de Investigación, Depto. de Fisicoquímica, Facultad de Ciencias Químicas, Benemérita Universidad Autónoma de Puebla, 22 sur y Av. San Claudio, Col. San Manuel, Puebla 72570, Mexico

⁵ Laboratorio de Estudios Cristalográficos, IACT, CSIC-UGR, Av. Las Palmeras nº4, 18100 Granada, Spain

* Correspondence: mareug.castro@correo.buap.mx (M.E.C.); enrique.gonzalez@correo.buap.mx (E.G.-V.); Tel.: +52-222-363-0623 (E.G.-V.)

Abstract: Citrulline (C₆H₁₃N₃O₃) is a non-protein amino acid found in watermelon. In physiological conditions, it is almost entirely present as a zwitterion, so its carboxylic and amine groups can act as Lewis donors, chelating metallic cations. In addition, Citrulline possesses a terminal ureide group of the aliphatic chain, which appears to be non-innocent. Although Citrulline is similar to other classical amino acids, only one coordination complex has been reported in the Cambridge Crystallographic Database. As part of our search for Casiopeina[®] analogs, we synthesized and characterized the copper bis-citrullinato complex, [Cu(Citr)₂]_n. The compound was described using UV-Vis, Infrared, and Raman spectroscopy, together with single-crystal X-ray diffraction. Computational tools were also used. The optimized structure, MEP map, IR and Raman spectra, and ¹H and ¹³C chemical shifts were obtained with functional mPW1PW91 using 6-31G(d) basis set for N, O, C, and H atoms, and LANL2DZ basis set and ECP=LANL2DZ for the Cu atom. TD-mPW1PW91 calculations generated the UV-Vis spectrum. Finally, AIM and Hirshfeld surface analysis were used to examine non-covalent interactions. Previous investigations suggest Casiopeina[®]-like complexes can interact with DNA/RNA, creating potential anticancer chemicals. The [Cu(Citr)₂]_n complex's polymeric nature and insolubility make it difficult for such purposes. However, the facile synthesis of D-Citrulline could be a novel way to find new applications for this interesting amino acid.

Keywords: Citrulline; copper; DFT calculations; Hirshfeld surface analysis; non-covalent interactions



Citation: Ramírez-Contreras, D.; García-García, A.; Sánchez-Gaytán, B.L.; Serrano-de la Rosa, L.E.; Melendez, F.J.; Choquesillo-Lazarte, D.; Rodríguez-Diéguez, A.; Castro, M.E.; González-Vergara, E. Bis-Citrullinato Copper(II) Complex: Synthesis, Crystal Structure, and Non-Covalent Interactions. *Crystals* **2022**, *12*, 1386. <https://doi.org/10.3390/cryst12101386>

Received: 6 September 2022

Accepted: 26 September 2022

Published: 29 September 2022

Publisher's Note: MDPI stays neutral with regard to jurisdictional claims in published maps and institutional affiliations.



Copyright: © 2022 by the authors. Licensee MDPI, Basel, Switzerland. This article is an open access article distributed under the terms and conditions of the Creative Commons Attribution (CC BY) license (<https://creativecommons.org/licenses/by/4.0/>).

1. Introduction

The discovery of Citrulline that we know today has been traditionally attributed to Mitsunori Wada in 1930, who separated and determined its chemical formula from the watermelon juice *Citrullus vulgaris* [1]. However, it was first isolated in 1914 by Yotaro Koga and Ryo Ohtake, although they did not describe its structure, nor did they name it [2]. Today, we know that L-Citrulline is also present in other foods, such as cucumbers, pumpkins, melons, squashes, and gourds [3].

L-Citrulline (C₆H₁₃N₃O₃) is not involved in protein formation since it is a non-essential amino acid. The body produces it endogenously, predominantly in the intestine [4,5], by biosynthesis from principally L-glutamine, L-arginine, and proline. During the urea cycle,

glutamine is transformed into ornithine, which is turned into L-Citrulline in the mitochondria. The second pathway uses arginine as a precursor to making Citrulline and nitric oxide; lastly, proline is metabolized into ornithine, which is converted into Citrulline [6]. Although this biomolecule has received little attention because it is non-protein, its complex metabolism has made it more relevant in recent decades [7]. It may be utilized as a biomarker or treatment for many diseases. If Citrulline metabolism is insufficient, the urea cycle and NO regulation do not work properly [8,9]. Citrulline supplementation may be used to treat hypertension since the NO cycle affects blood pressure, arginine shortage, liver damage, or cerebral malaria [10–13]. In addition, the consumption of Citrulline could also be beneficial in the treatment and prevention of other important disorders such as erectile dysfunction, sickle cell anemia, cancer chemotherapy, and cardiovascular disease; to enhance protein content in malnourished and elderly patients; or to treat Alzheimer's disease and multi-infarct dementia, among others [14,15]. Another research points out the role of Citrulline as an antibody to citrullinated peptides. Protein citrullination could produce, as the final step, autoantibodies which can be used as biomarkers in various disorders such as rheumatoid arthritis, intestinal pathology, and short bowel syndrome [16]. It is clear that Citrulline plays a critical role in human health. Still, much more investigation is needed before Citrulline is used in therapy with confidence against all mentioned disorders [17].

Coordination complexes based on biological ligands and d block metal ions, such as Cu(II), Co(II), and Zn(II), have several applications in environmental, biological, pharmaceutical, and chemical and electrochemical industries [18]. In 1938, Fox S. reported the preparation of Citrulline from hydrolysis of arginine. In this procedure, copper oxide was introduced to form the copper-Citrulline complex, which serves as an intermediate for the isolation of Citrulline after the copper was removed; thus, the copper complex was mentioned for the first time [19]. In the same year, Kurtz described the synthesis of DL-Citrulline, proposed the compound's structure, and mentioned its insolubility [20]. Trikha et al., (1968) and Clarke and Martell (1970) reported the formation constants for 1:1 and 1:2 molar ratio Cu(II)-Citrulline complexes in aqueous solutions [21,22]. Later, Yamauchi et al., crystallized [Cu(L-His)(L-Citr)] complex in 1979 [23], and Ganadu et al., examined Pd(II)-Citrulline interaction using ^1H and ^{13}C NMR spectroscopy and potentiometry in 1991 [24]. The [Pd(Citr) $_2$] complex was subsequently synthesized and characterized by Mascaliovas et al., (2015). Its crystal structure was solved by powder X-ray diffraction data and simulated annealing in real space [25]. The structure showed Pd(II) ions in a roughly square planar environment and deprotonated Citrulline. Finally, equilibrium studies of Hg(II)—L-Citrulline(A)—Uracil (B) with d-block metal ions M = Cu(II), Zn(II), Co(II), and Ni(II) were reported in 2017 [26]. The same group recently explored the equilibrium constants of Citrulline/tryptophan and thymine with Cu(II), Zn(II), Co(II), and Ni(II) [27].

As part of our attempts to generate possible metallodrugs based on Casiopeina[®] analogs, we have previously reported copper-mixed complexes incorporating lysine, ornithine, and glutamine, and docking studies reveal their interaction with DNA/RNA [28–30]. Here we report the synthesis and experimental-theoretical characterization of the [Cu(Citr) $_2$] complex and its crystal structure for the first time. In addition to the complete structural characterization by spectroscopic techniques, DFT studies and Hirschfeld analysis have been carried out to describe important electronic and structural characteristics such as relevant non-covalent interactions.

2. Materials and Methods

2.1. Synthesis of [Cu(Citr) $_2$] $_n$

L-Citrulline (C $_6$ H $_{13}$ N $_3$ O $_3$; M.W. = 175.188 g/mol) was purchased from Merck Mexico, while copper chloride (II) dihydrate (CuCl $_2$ ·2H $_2$ O; M.W. = 170.480 g/mol), copper nitrate (II) trihydrate Cu(NO $_3$) $_2$ ·3H $_2$ O; M.W. = 241.600 g/mol), and copper perchlorate (II) hexahydrate Cu(ClO $_4$) $_2$ ·6H $_2$ O; M.W. = 370.540 g/mol) were purchased from Sigma-Aldrich. Methanol (CH $_3$ OH) and deuterated water (D $_2$ O) (99.9%) were purchased from Fisher Scientific (J.K. Baker). Purification or pretreatment of reagents was not necessary.

The bis-citrullinato copper (II) complex was synthesized using a similar methodology described by Su et al. [31]. In a flask, 2 mmol (0.340 g) of Citrulline was mixed with 1 mmol of $\text{CuCl}_2 \cdot 2\text{H}_2\text{O}$ (0.170 g) in 10 mL of methanol. The mixture was stirred for two hours (due to the low solubility of Citrulline in methanol) under slight heating (the temperature shall not exceed 50 °C). Then, 2 mmol of sodium hydroxide (0.080 g) dissolved in methanol (10 mL) was added, and the mix continued to be stirred in the same conditions for 2 h until a deep blue powder was formed. After this process, the suspension was filtered using a Whatman 40 filter paper, and the solid was washed with methanol and air-dried at room temperature. Yield of $[\text{Cu}(\text{Citr})_2]$: (0.358 g) 68.89%. The same procedure was repeated separately using $\text{Cu}(\text{NO}_3)_2 \cdot 3\text{H}_2\text{O}$ and $\text{Cu}(\text{ClO}_4)_2 \cdot 6\text{H}_2\text{O}$; a blue solid with the same IR spectrum was obtained regardless of the copper salt used.

The same compound was obtained by electrosynthesis to give good quality crystals [32,33]. A piece of standard copper wire was used as a sacrificial anode, a pencil carbon electrode as a cathode, and an AC eliminator was used as a power supply. In this case, 5.0 mmol of Citrulline was dissolved in 50 mL of water, and this solution was used as an electrolyte. The conditions were fixed to 2 A and 9 V. The electrosynthesis was carried out for 6–10 h or until the formation of crystals in the copper anode. The resulting crystals were separated from the anode, washed with methanol, and air-dried at room temperature. The new compound was fully characterized by single-crystal X-ray diffraction and spectroscopic techniques.

2.2. Characterization Methods

The UV-Vis experiment was performed in a Cary 5000 UV-Vis-NIR Spectrophotometer-Agilent. A powder holder was used to compensate for the very small amount, and a Teflon tablet with a cavity was used to deposit the material. The scanning was performed from 200 to 800 nm, at a scanning speed of 600 nm per minute, with 1 nm steps in the reflectance mode. The accessory used is the DRA-2500 with an internal PbS detector. The Infrared spectrum was recorded from 4000 to 650 cm^{-1} using a Nicolet 6700 FTIR spectrophotometer coupled with the iTR accessory with a diamond tip. The Raman spectrum was obtained at room temperature in a backscattering configuration using the 633 nm line of a He-Ne laser as an excitation source by using a LabRAM HR-Olympus Micro Raman. The ^1H - and ^{13}C -NMR spectra were recorded by adding 10 mg of the blue powder in 500 μL of D_2O and 50 μL of HCl 1M to enhance the compound's solubility using a Bruker AVANCE III 500 MHz spectrometer at 25 °C. Quality crystals of the copper-Citrulline complex were subject to X-ray diffraction studies. Data were collected with a Bruker D8 Venture diffractometer with a Photon detector equipped with graphite monochromated CuK radiation ($\lambda = 1.54178 \text{ \AA}$). The data were processed with the APEX3 suite, and SADABS-2016/2 was used for absorption correction [34]. The structure was solved by direct methods using the ShelXT program and refined by full-matrix least squares on F^2 with SHELXL-2019 [35]. The positional and anisotropic atomic displacement parameters were refined for all non-hydrogen atoms. Hydrogen atoms were located in different Fourier maps and included as fixed contributions riding their parent atoms with isotropic thermal factors chosen as 1.2 times their carrier atoms. The OLEX2 software [36] was used as a graphical interface. Details of the structure determinations and refinement are summarized in Table 1 and Tables S1–S3 in the Supplementary Materials Section. Crystallographic data (excluding structure factors) for the structure reported in this paper have been deposited with the Cambridge Crystallographic Data Center as supplementary publication No. 2172421. Copies of the data can be obtained free of charge on application to the Director, CCDC, 12 Union Road, Cambridge, CB2 1EZ, UK (Fax: +44-1223-335033; e-mail: deposit@ccdc.cam.ac.uk or <http://www.ccdc.cam.ac.uk> (accessed on 12 July 2022)).

Table 1. Experimental details of the X-ray collection of data.

	[Cu(Citr) ₂] _n
Chemical formula	C ₁₂ H ₂₄ CuN ₆ O ₆
Formula weight (g mol ⁻¹)	411.91
CCDC	2,172,421
Crystal system	Monoclinic
Space group	<i>P</i> 2 ₁
Temperature (K)	300.7
a, b, c (Å)	5.1270 (2), 9.2086 (4), 17.1099 (7)
β (°)	93.972 (2)
V (Å ³)	805.86 (6)
Z	2
Radiation type	Cu Kα (1.54178 Å)
ρ _{calcd} (g cm ⁻³)	1.698
μ (mm ⁻¹)	2.339
Crystal size (mm)	0.12 × 0.1 × 0.1
GoF on F ²	1.147
R ₁ [I > 2σ(I)]	0.0497
R ₁ [all data]	0.0512
wR ₂ [I > 2σ(I)]	0.1469
wR ₂ [all data]	0.1520

2.3. Computational Details

Density functional theory (DFT) [37] and time-dependent DFT (TD-DFT) [38] calculations were used to obtain the optimized structure and the electronic properties of the compound [Cu(Citr)₂]_n in both its electronic ground and excited states. The functional mPW1PW91 [39] with the split-valence 6-31G(d) basis set [40] was used for the C, H, O, and N atoms. The LANL2DZ basis set [41] and an effective core potential (ECP) were used for the copper atom (mPW1PW91/6-31G(d)-LANL2DZ and ECP=LANL2DZ). Calculations were performed without symmetry imposition. The vibrational frequencies were determined to establish the stationary points on the potential energy surface, using the second derivatives of the energy analytically. The solvent effect was implicitly included with the universal solvation model based on solute electron density (SMD) [42], using water as solvent. This theory level was used to calculate geometry optimization, the molecular electrostatic potential (MEP) map, IR and Raman, and ¹H and ¹³C NMR spectra calculations. For IR and Raman, calculated spectra were obtained with a scaling factor of 0.961. The ¹H and ¹³C NMR spectra were calculated using the Gauge-Independent Atomic Orbital (GIAO) method [43]. For the UV-Vis spectrum, TD-mPW1PW91 time-dependent density functional and the same basis set was applied to the vertical absorption calculation. It is a reliable tool used to investigate excited states of medium and large molecular systems with reasonable computational cost [37]. The calculations were carried out with the Gaussian16 program [44], and the results were visualized with the GaussianView 6.0.16 program [45]. The main non-covalent interactions were characterized by mPW1PW91/6-31G(d)-LANL2DZ wavefunction using the atoms in molecules (AIM) approach with AIMAll software [46]. Finally, the Hirshfeld surface analysis was performed from the crystallographic data using CrystalExplorer 17.5 software [47].

3. Results

3.1. Structural Description

[Cu(Citr)₂]_n crystallizes in the monoclinic *P*2₁ space group and consists of a bi-dimensional coordination polymer. The asymmetric unit comprises one Cu(II) ion and two coordinated Citrulline ligand molecules, being the X-ray formula [Cu(Citr)₂]_n (Figure 1a). Each metal center exhibits an octahedral geometry with an elongated deformation and coordinates to four Citrulline molecules. The CuO₄N₂ sphere is formed by two O1 atoms from the carboxylate groups of ligands A and B, two N1 atoms belonging to amino groups

of the same ligands, and two O3 atoms of amide groups of two different ligands (Figure 1b). The coordination sphere's deformation results from the high Jahn–Teller effect around *d*-orbitals of Cu(II) in octahedral geometry, which tend to split degenerate energy levels [48]; the basal positions are occupied by two Cu–N and two Cu–O bonds with distances in the range of 1.952(8)–1.978(8) Å and 1.951(8)–1.961(7) Å, respectively, similar to other reported structures [30,49–51]. According to the literature, the Cu–O bond distances at the apical positions range from 2.4 to 2.8 Å, corresponding to electrostatic interactions [52]. In our case, Cu–O3Aⁱ (*i* = 1 – *x*, –1/2 + *y*, –*z*) and Cu–O3Bⁱⁱ (*ii* = –*x*, 1/2 + *y*, 1 – *z*) 2.724(9) and 2.622(9) Å, respectively.

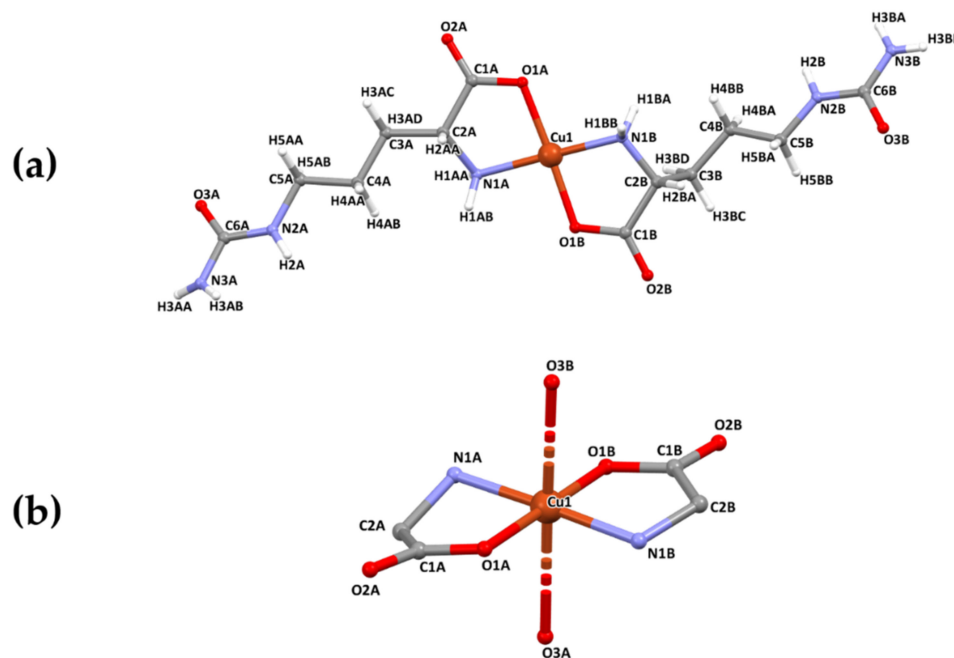


Figure 1. (a) Asymmetric unit of [Cu(Citr)₂]_n. (b) Detail of the coordination sphere. Color code: copper (brown), oxygen (red), nitrogen (blue), carbon (grey), and hydrogen atom (white).

The Citrulline molecule acts as a ditopic-bringing linker since carboxylate, amino, and amide groups interact with two metallic ions. The O1 atom of carboxylate and N1 from primary amine coordinate to one Cu(II) ion by a bidentate mode, as proposed for similar structures with Co(II), Cu(II), Pd(II), and Zn(II) already published [25,53,54]. However, for the first time, in this structure, the oxygen O3 of the amide group is also coordinated to one metal ion and forms the octahedron's axial bond. Moreover, it is essential to note that the reagent used in the synthesis was the L isomer of Citrulline. In contrast, the complex obtained gives rise to the D-Citrulline enantiomers due to the coordination with Cu(II) (Figures S1–S4). This arrangement of the ligands gives rise to layers parallel to the [202] plane (Figure 2).

In addition, the supramolecular structure is stabilized by intra- and intermolecular hydrogen bonds of type N–H···O (Figure 3 and Table 2). Within the layers, two main hydrogen bonds that were analyzed by computational tools are formed from the primary and secondary amine to the oxygen of the carboxylate group of a different ligand, giving rise to a *R*₂¹(6) and *R*₂²(8) graph-set motives, according to Etter's nomenclature [55] (Figure 3).

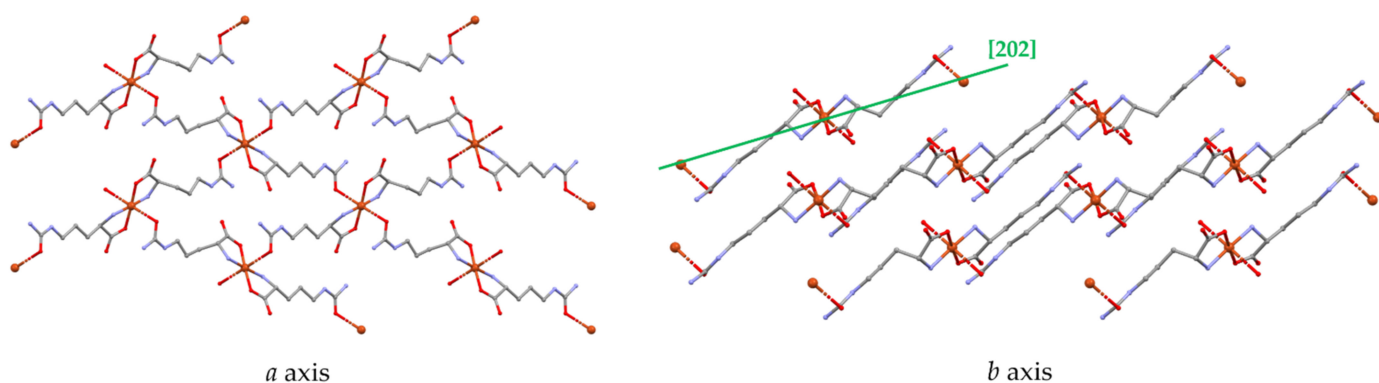


Figure 2. Crystal structure of the compound $[\text{Cu}(\text{Citr})_2]_n$ along a and b crystallographic axis. The plane $[202]$ is shown in green color. Hydrogen atoms have been omitted for clarity.

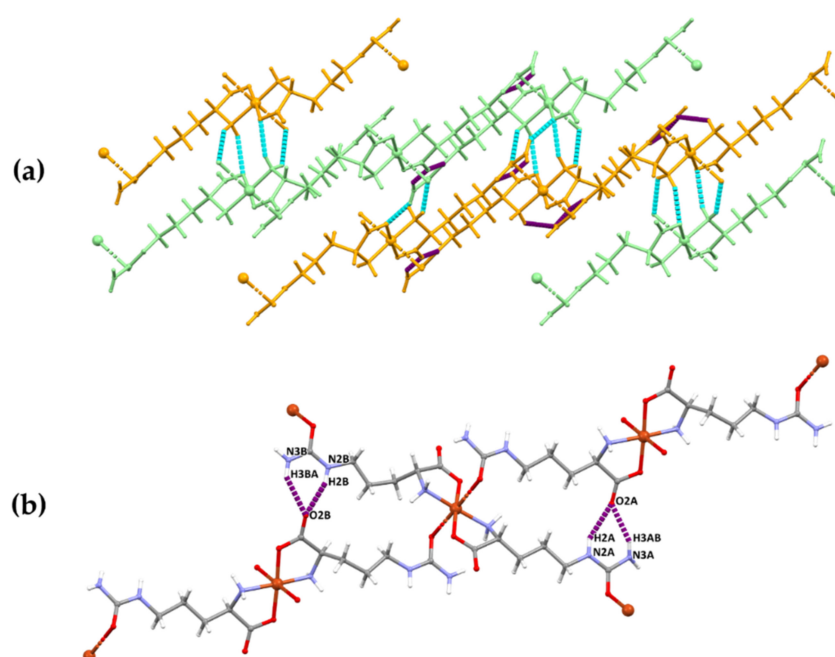


Figure 3. (a) Perspective view of all the hydrogen bonds in the structure. The different layers are indicated in orange and light green color, while intra- and intermolecular hydrogen bonds are in light blue and purple dotted lines, respectively. (b) Detail of the intramolecular H-bonds, which gives rise to a $R_2^1(6)$ and $R_2^2(8)$ ring motives.

Table 2. Hydrogen bonds for compound $[\text{Cu}(\text{Citr})_2]_n$.

D-H...A	D-H (Å)	H...A (Å)	D-H...A (Å)	Angle (°)
N2A-H2A...O2A ⁱ	0.86	2.17	2.955(14)	150.9
N3A-H3AB...O2A ⁱ	0.87	2.14	2.935(16)	151.6
N2B-H2B...O2B ⁱⁱ	0.86	2.02	2.840(14)	159.1
N3B-H3BA...O2B ⁱⁱ	0.86	2.26	2.997	144.1
N1A ⁱⁱⁱ -H1AA...O1A	0.89	2.34	3.153	151.7
N1A ^{iv} -H1AB...O3A	0.89	2.22	2.996	145.6
N3B ^v -H3BB...O1A	0.86	2.07	2.928(12)	171.4
N3A-H3AA...O1B ^{iv}	0.88	2.26	3.047	148.7

Symmetry operations: ⁱ = $1 - x, \frac{1}{2} + y, -z$; ⁱⁱ = $-x, \frac{1}{2} + y, 1 - z$; ⁱⁱⁱ = $-1 + x, y, z$; ^{iv} = $2 - x, \frac{1}{2} + y, -z$; ^v = $-1 - x, \frac{1}{2} + y, 1 - z$.

The selected parameters for the complex $[\text{Cu}(\text{Citr})_2]$ are shown in Table 3 for comparison between X-ray data and the calculated structure obtained at the level of theory mPW1PW91/6-31G(d)-LANL2DZ and ECP=LANL2DZ. The numbering convention is in agreement with Figure 1a. Similar values are observed in the bond lengths and angles. Some dihedral angles, such as C1B–C2B–N1B–Cu1 and C2B–C3B–C4B–C5B, present the major differences between the X-ray and the calculated data with 9 and 16°. Both in the X-ray data and the calculated data, the non-symmetrical structure of each Citrulline can be observed in the complex. In addition, according to the parameters around the equatorial positions of the atoms coordinated to the Cu ion, a distorted octahedral geometry is observed. The agreement between the optimized structure and that obtained with X-ray diffraction can be clearly observed in Figure 4, where both complexes were fitted using VMD molecular graphics viewer [56]. Only, small differences can be observed with an RMSD calculated value of 0.24 between them.

Table 3. Selected X-ray and optimized parameters for the compound $[\text{Cu}(\text{Citr})_2]$ obtained at the level of theory mPW1PW91/6-31G(d)-LANL2DZ and ECP=LANL2DZ. Bond lengths in (Å) and angles in (°).

Parameter	X-ray Data	Calculated
Cu1–O1A/Cu1–O1B	1.974/1.940	1.978/1.965
Cu1–N1A/Cu1–N1B	1.993/1.958	2.018/2.027
O1A–C1A/O1B–C1B	1.271/1.286	1.290/1.290
C1A–O2A/C1B–O2B	1.231/1.217	1.237/1.237
C1A–C2A/C1B–C2B	1.529/1.531	1.535/1.531
N1A–C2A/N1B–C2B	1.502/1.461	1.474/1.474
C2A–C3A/C2B–C3B	1.528/1.541	1.523/1.533
C3A–C4A/C3B–C4B	1.501/1.516	1.525/1.527
C4A–C5A/C4B–C5B	1.525/1.477	1.520/1.522
C5A–N2A/C5B–N2B	1.476/1.429	1.450/1.447
O1A–Cu1–N1B/O1B–Cu1–N1A	96.91/94.43	98.00/96.07
C1A–O1A–Cu1/C1B–O1B–Cu1	113.46/115.04	114.95/115.43
C2A–N1A–Cu1/C2B–N1B–Cu1	104.76/110.23	106.74/108.31
O1A–C1A–C2A/O1B–C1B–C2B	116.38/116.54	115.56/116.86
O2A–C1A–O1A/O2B–C1B–O1B	123.16/123.33	123.90/124.08
C2A–C3A–C4A/C2B–C3B–C4B	112.72/116.79	112.26/115.66
C3A–C4A–C5A/C3B–C4B–C5B	110.52/116.08	112.72/114.08
C4A–C5A–N2A/C4B–C5B–N2B	111.02/112.14	109.92/109.49
C1A–O1A–Cu1–N1A/C1B–O1B–Cu1–N1B	12.41/–10.77	13.22/–10.06
O2A–C1A–O1A–Cu1/O2B–C1B–O1B–Cu1	–173.90/–177.11	–177.30/179.08
C1A–C2A–N1A–Cu1/C1B–C2B–N1B–Cu1	40.41/–17.16	36.87/–26.97
C1A–C2A–C3A–H3AC/C1B–C2B–C3B–H3BC	–53.01/–51.68	–48.62/–50.53
C2A–C3A–C4A–C5A/C2B–C3B–C4B–C5B	176.50/81.02	177.12/65.95
C3A–C4A–C5A–N2A/C3B–C4B–C5B–N2B	176.51/174.14	–178.41/178.61

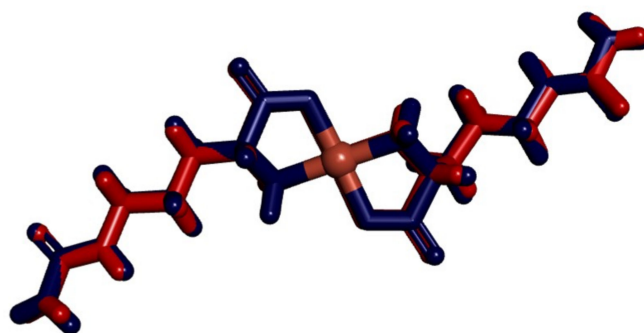


Figure 4. View of the X-ray complex and the optimized complex of $[\text{Cu}(\text{Citr})_2]$ fitted. X-ray complex is shown in red and calculated complex in blue.

3.2. Characterization of the Complex

3.2.1. UV-Visible Spectroscopy

Visible spectra of copper complexes with aminoacidato reveal a $d-d$ transition as a broad band with a maximum of 650–550 nm and two lower-intensity bands at 540 and 720 nm—such an attribute for a square planar CuO_2N_2 chromophore. For the compound obtained, a typical unsymmetrical band at 600 nm was obtained by diffuse reflectance due to the insolubility of the complex. It corresponds to a $d-d$ transition due to the coordination of two aminoacidato ligands and two carbonyl oxygens of the ureide groups comprising a tetragonally distorted octahedral environment (Figure 5). The $d-d$ band consists of three overlapping electronic dipole transitions which are related to the three spin-allowed transitions, ${}^2A_{1g}(dz^2) \rightarrow {}^2B_{1g}(dx^2-y^2)$, ${}^2E_g(dyz \approx dxz) \rightarrow {}^2B_{1g}(dx^2-y^2)$, and ${}^2B_{2g}(dxy) \rightarrow {}^2B_{1g}(dx^2-y^2)$, respectively, for a distorted octahedral geometry of the copper(II) ion. The $n \rightarrow \pi^*$ characteristic band in the UV spectra at 267 nm is assigned to the intra-ligand transition of the amide C=O bond [57–62].

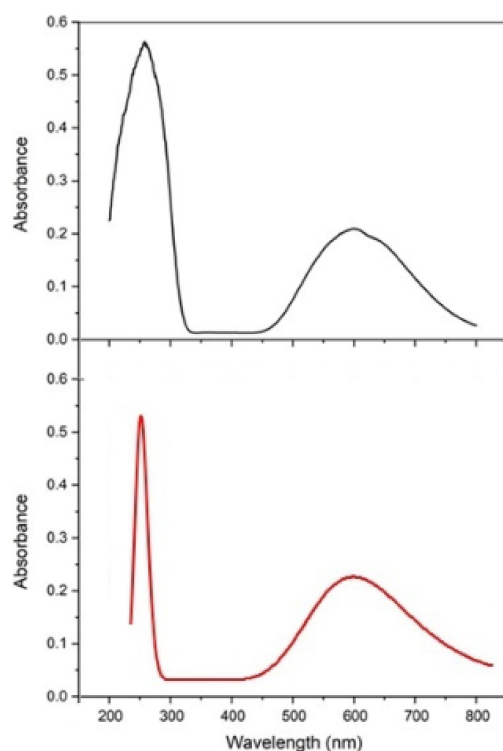


Figure 5. UV-Vis experimental spectrum of $[\text{Cu}(\text{Citr})_2]_n$ obtained by diffuse reflectance (black line) and calculated spectrum at the level of theory mPW1PW91/6-31G(d)-LANL2DZ and ECP=LANL2DZ (red line).

The theoretical UV-Vis absorption spectrum of $[\text{Cu}(\text{Citr})_2]_n$ was calculated using the TD-mPW1PW91 functional. The 6-31G(d)-LANL2DZ basis sets and the ECP=LANL2DZ for the Cu atom were used. The solvent effect was included using the SMD model with water as solvent. This UV-Vis spectrum was compared with the experimental one measured from 200 to 800 nm (Figure 5). Values such as absorption wavelengths, λ_{exp} and λ_{theo} , excitation energies, E_{exc} , oscillator strengths, and significant contributions of the electronic transitions were calculated using twenty states ($n_{\text{states}} = 20$).

Table 4 shows a good agreement between the experimental measurements and calculated values using the TD-DFT methodology. The experimental absorption band of $[\text{Cu}(\text{Citr})_2]_n$ in the solid state is observed at 267 nm, corresponding to the $n \rightarrow \pi^*$ transition, which is calculated at 253 nm with the fundamental contribution of the HOMO and LUMO orbitals. The broadest band, which appears at 420–800 nm, is assigned to $d \rightarrow d$ transitions. This band shows two shoulders, the first between 523 (511 nm) and the second between 665

(642 nm). Both were found with low intensity and low contribution of the frontier molecular orbitals. Finally, the maximum of this broadband was calculated between 600 and 592 nm, with maximum intensity at 600 nm, in good agreement with the reported values. The TD-mPW1PW91 functional provided reliable results for the electronic transitions and excitation energies of compound $[\text{Cu}(\text{Citr})_2]_n$ (see Figure 5 and Table 4). Due to that, the complexes of Cu(II) have one unpaired electron, located at the molecular orbitals β , and it is responsible for the electronic transitions. Only its spin was considered to analyze the UV-Vis spectrum. The mPW1PW91/6-31G(d)-LANL2DZ and ECP=LANL2DZ level of theory was used to calculate the gap energy, which corresponds to the difference between the Highest Occupied Molecular Orbital (HOMO) and the Lowest Unoccupied Molecular Orbital (LUMO). Therefore, the calculated value of the energy gap is 4.54 eV, using the UmPW1PW91 functional. On the other hand, a small energy gap value indicates good electronic conduction. Thus the electronic transitions between HOMO and LUMO are easy to carry out.

Table 4. Experimental absorption wavelengths (λ_{exp}), calculated absorption wavelengths (λ_{theo}), excitation energies (E_{exc}), oscillator strengths, and significant contributions of the electronic transitions of $[\text{Cu}(\text{Citr})_2]_n$ calculated at the level of theory mPW1PW91/6-31G(d)-LANL2DZ and ECP=LANL2DZ.

λ_{exp} (nm)	λ_{theo} (nm)	E_{exc} (eV)	Osc. Strengths	Major Contributions
720	665	1.87	0.0001	H-6→L+1 (2%)
	651	1.90	0.0003	H-8→L (4%)
	642	1.93	0.0003	H-4→L (3%)
600	600	2.06	0.0223	H→L (95%)
	598	2.07	0.0105	H-4→L (55%)
	592	2.09	0.0009	H-1→L (75%)
540	523	2.37	0.0003	H-8→L+1 (3%)
	516	2.40	0.0005	H-6→L+1 (2%)
	511	2.43	0.0001	H-2→L+1 (5%)
267	253	4.90	0.0436	H→L (91%)

3.2.2. Infrared Spectroscopy

The Infrared spectrum of the synthesized complex is presented in Figure 6, and it has three important band assignments; the first one refers to the peaks in the region of 3450–3150 cm^{-1} that are mainly attributed to amide (NH_2) asymmetric and symmetric stretching, amide (NH) stretching, and asymmetric and symmetric stretching vibrations of the amino group; the second one refers to two nearby weak peaks in the 2900–2800 cm^{-1} region, which correspond to asymmetric and symmetric vibrations of the methylene groups of the hydrocarbon chain. The third set of assignments corresponds to the region of 1700–1350 cm^{-1} . The peaks at 1652 and 1636 cm^{-1} correspond to C=O stretching vibrations of the carbonyl and carboxyl groups, respectively. The intense bands at 1575 and 1549 cm^{-1} correspond to scissoring vibrations of the (NH_2) amino and amide groups, respectively, and the peak at 1385 cm^{-1} is attributed to carboxylate symmetric stretching. The three assignments are concordant to a coordinated aminoacidato structure [25,63,64].

The theoretical IR vibrational frequencies of $[\text{Cu}(\text{Citr})_2]_n$ are shown and compared with the experimental measurements obtained in this work presented in Table 5. In the high-frequency region at 3500–3400 cm^{-1} , the peaks are assigned to the stretching vibrational modes of the amide and amino groups (see Figure 6). In Table 5, it is possible to observe that the experimental values for other complexes of Pd(II) and Cu(II) with different ligands found in this region are in good agreement with those obtained experimentally and theoretically in this work. In addition, the double band assigned to the asymmetric and symmetric stretching modes, $\nu_{\text{asym}}(\text{CH}_2)$ and $\nu_{\text{sym}}(\text{CH}_2)$, of the methylene groups are found in the region 2951–2904 cm^{-1} . A low-intensity signal experimentally observed at 1652 cm^{-1} , corresponding to the stretching mode of the carbonylic group $\nu(\text{C}=\text{O})$, is theoretically assigned by DFT calculations at 1708 cm^{-1} . The region 1700–1350 cm^{-1} at

the experimental spectrum is relatively challenging to assign. However, with the help of theoretical calculations, three different vibrational modes can be observed. The first corresponds to the stretching modes of the carboxylic group, $\nu_{\text{asym}}(\text{O}=\text{C}-\text{O}^-)$, at 1695 cm^{-1} . The second is associated with the scissoring modes of amide $\delta(\text{NH}_2)$ and amino $\delta(\text{NH}_2)$ groups at 1583 and 1559 cm^{-1} , respectively. The third vibrational mode is assigned to the symmetric stretching of the carboxylic group, $\nu_{\text{sym}}(\text{O}=\text{C}-\text{O}^-)$, at 1390 cm^{-1} . A large displacement between the bands of asymmetric and symmetric modes of the carboxylic group is observed ($\Delta\nu_{\text{complex}} = 305\text{ cm}^{-1}$), which suggests monodentate coordination of the carboxylate group through an oxygen atom. On the other hand, the metal-ligand vibrational modes are difficult to assign, however using DFT calculations and comparing with previous studies, it was possible to perform an adequate assignation of the stretching modes (Cu–N) in the higher frequency region than that region for stretching modes (Cu–O) calculated at 391 cm^{-1} in this work. The stretching mode $\nu(\text{Cu}-\text{N})$ was calculated at 576 cm^{-1} , which is in good agreement with the values for some complexes of Cu(II) and Pd(II) with different amino acids reported in previous studies [24,25,62].

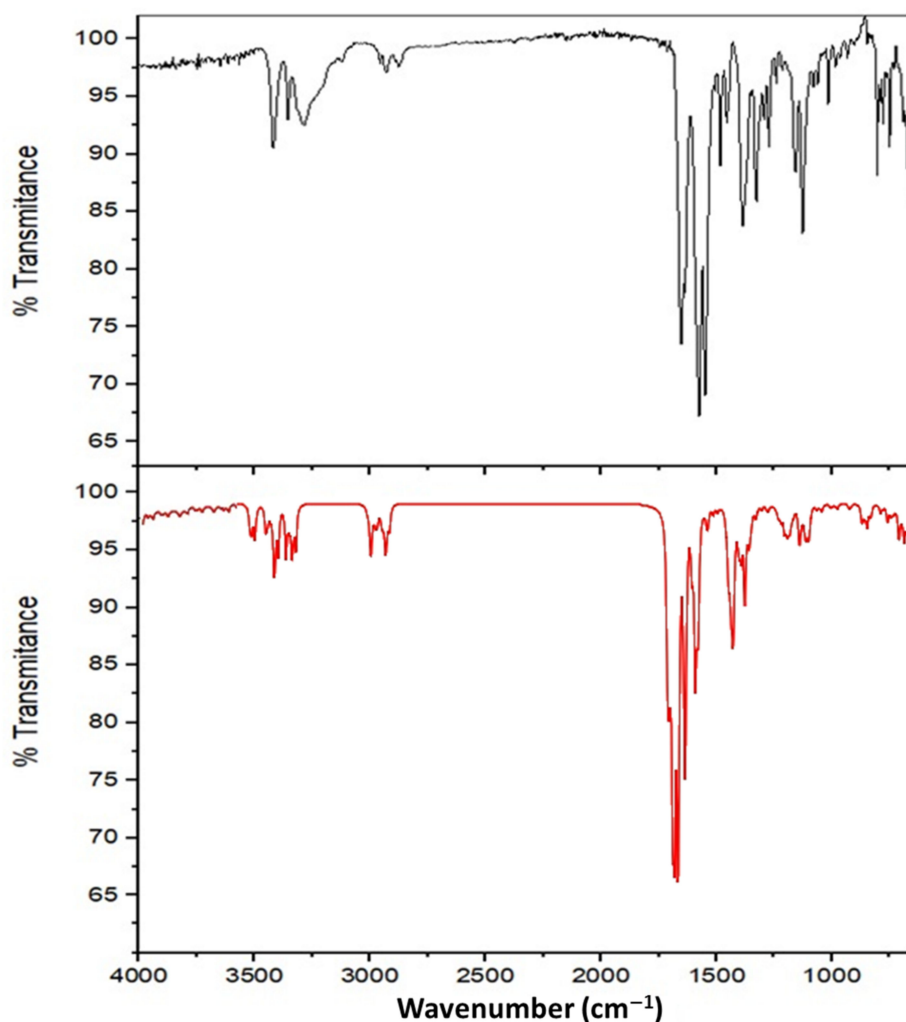


Figure 6. FTIR experimental spectrum of $[\text{Cu}(\text{Citr})_2]_n$ in the region $4000\text{--}650\text{ cm}^{-1}$ (black line) and FTIR calculated spectrum at the level of theory mPW1PW91/6-31G(d)-LANL2DZ and ECP=LANL2DZ (red line).

Table 5. FTIR experimental vibrational frequencies of $[\text{Cu}(\text{Citr})_2]_n$ and FTIR calculated vibrational frequencies obtained at the level of theory mPW1PW91/6-31G(d)-LANL2DZ and ECP=LANL2DZ.

Experimental (cm^{-1})	mPW1PW91 (cm^{-1})	Assignments
3450	3501	$\nu_{\text{asym}}(\text{NH}_2)$ amide
	3438	$\nu_{\text{sym}}(\text{NH}_2)$ amide + $\nu_{\text{sym}}(\text{NH})$ amide
	3416	$\nu_{\text{sym}}(\text{NH}_2)$ amide
	3415	$\nu_{\text{asym}}(\text{NH}_2)$ amino
	3330	$\nu_{\text{sym}}(\text{NH}_2)$ amino
3150	2951	
	2947	$\nu_{\text{asym}}(\text{CH}_2)$
	2909	
2900	2910	
	2904	$\nu_{\text{sym}}(\text{CH}_2)$
2800	1708	$\nu(\text{C}=\text{O})$ carboxylic group
1652	1695	$\nu_{\text{asym}}(\text{O}=\text{C}-\text{O}^-)$ carboxylic group
1636	1583	$\delta(\text{NH}_2)$ amide
1575	1559	$\delta(\text{NH}_2)$ amino
1549	1390	$\nu_{\text{sym}}(\text{O}=\text{C}-\text{O}^-)$ carboxylic group
1385	576	$\nu(\text{Cu}-\text{N})$

3.2.3. Raman Spectroscopy

The Raman spectrum is presented in Figure 7. The band at 3276 cm^{-1} is broadband, comprising all NH stretching frequencies of the amide and amino nitrogens. The most intense peak corresponds to the symmetric vibration of the terminal NH_2 of the amide group. The bands at 2924, 2910, 2895, 2881, and 2874 cm^{-1} are congruent with the bonds in the amino acid chain of carbons (CH_{str} , β , γ , δ). Between them, the peaks at 2924, 2910, and 2881 cm^{-1} present a slight shift with respect to the spectrum of pure Citrulline, which could be associated with the presence of Cu(II). The band at 1684 cm^{-1} appears minimized and corresponds to the $\text{C}=\text{O}$ of the carboxylate. The peaks at 1463, 1460, 1327, and 1297 cm^{-1} coincide with those reported for L-Citrulline for CH_2 scissor, and at 1127, 990 cm^{-1} for CH twist. The band at 1453 cm^{-1} is associated with the CH_2 bend, 1312 cm^{-1} is associated with the wiggle of CH_2 , 1279 cm^{-1} can be identified with the twisting of CH_2 , 682 cm^{-1} belongs to the COO bend, 567 cm^{-1} associates with the C-O bond rocking in the carboxyl plane and 289 cm^{-1} is associated with a rocking C-C bond [65–70].

The experimental and the theoretical Raman vibrational frequencies of $[\text{Cu}(\text{Citr})_2]_n$ are collected in Table 6. In the same way as the IR analysis, the theoretical Raman spectrum is in good agreement with experimental values obtained in this work and with values previously reported by Baran et al., for complexes of Cu(II) with different amino acids [64]. The stretching mode of the hydrogen linked to C_α , $\nu(\text{C}_\alpha\text{H})$, is theoretically assigned at about 2932 cm^{-1} . In addition, the stretching mode $\nu(\text{C}-\text{N})$ of the amino group is calculated at the $1189\text{--}1163 \text{ cm}^{-1}$ region, which is in agreement with other values reported (see Table 6). The Raman vibrational bands observed in Figure 7 in the region at $3330\text{--}2894 \text{ cm}^{-1}$ correspond to pure symmetric modes of the amino group $\nu_{\text{sym}}(-\text{NH}_2)$ and $\nu_{\text{sym}}(\text{CH}_2)$ and $\nu_{\text{sym}}(\text{CH})$ modes of the hydrocarbon chain. In addition, the symmetric modes for the carboxylic and carboxylic groups are pure vibrational modes found in the $1642\text{--}1436 \text{ cm}^{-1}$ range. A coupled mode corresponding to the scissoring mode, $\delta(\text{CH}_2)$, of the hydrocarbon chain coupled with the stretching mode of the carboxylic group, $\nu(\text{O}=\text{C}-\text{O}^-)$, was calculated at the $1354\text{--}1307 \text{ cm}^{-1}$ range.

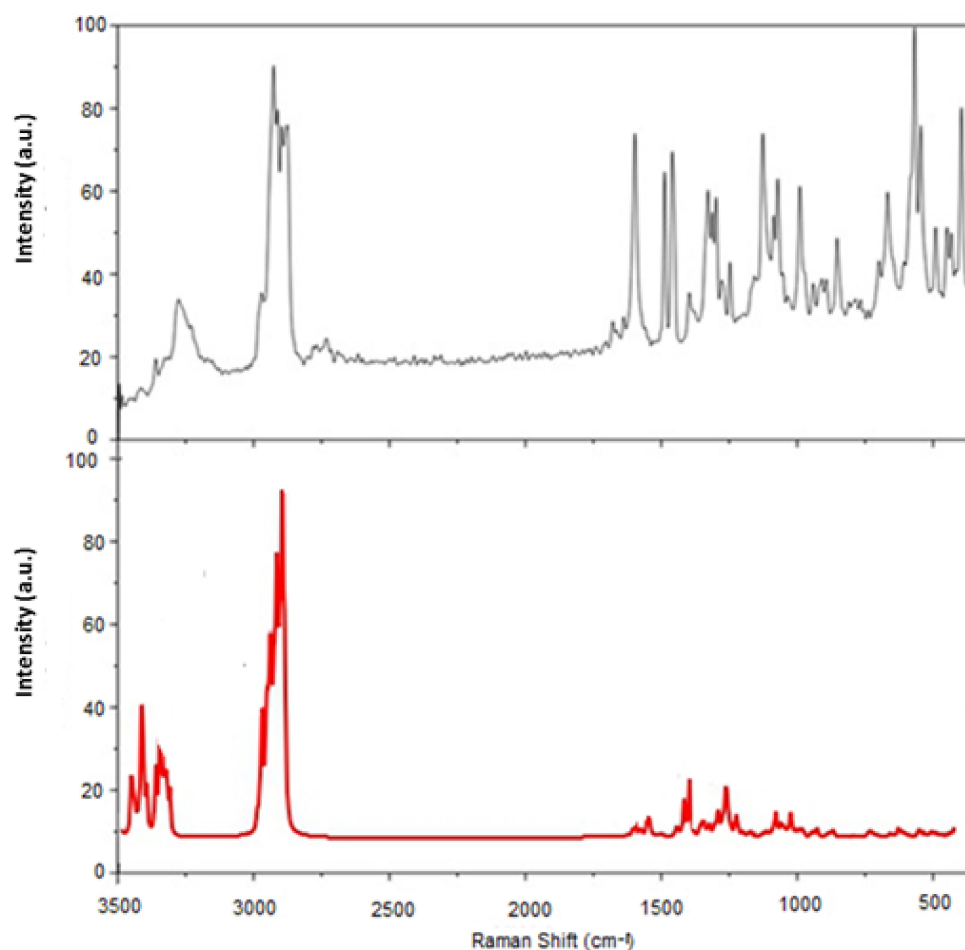


Figure 7. FT-Raman experimental spectrum of $[\text{Cu}(\text{Citr})_2]_n$ in the region $3500\text{--}450\text{ cm}^{-1}$ (black line) and FT-Raman calculated spectrum at the level of theory mPW1PW91/6-31G(d)-LANL2DZ and ECP=LANL2DZ (red line).

Table 6. FT-Raman experimental and calculated vibrational frequencies of $[\text{Cu}(\text{Citr})_2]_n$ obtained at the level of theory mPW1PW91/6-31G(d)-LANL2DZ and ECP=LANL2DZ.

Experimental	mPW1PW91	Assignments
3276	3330	$\nu_{\text{sym}}(-\text{NH}_2)$ amino
	2935–2929	$\nu(\text{C}_\alpha\text{H})$
2924, 2910	2927, 2913	$\nu(\text{CH}_2)$
2895, 2881, 2874	2902–2894	$\nu(\text{CH})$
1684	1642–1619	$\nu(\text{C}=\text{O})$ amide
1463–1460	1465–1436	$\nu(\text{C}=\text{O})$ carboxylic group
1327–1297	1354–1307	$\delta(\text{CH}_2) + \nu(\text{O}=\text{C}-\text{O}^-)$
1127	1189–1163	$\nu(\text{C}-\text{N})$ amino

3.2.4. NMR Studies

In Figure 8, the NMR spectra of ^1H and ^{13}C of the paramagnetic copper(II) complex and free Citrulline are presented. Tetramethylsilane (TMS) was the reference to measure both spectra. According to the literature, the unpaired electron in Cu(II) complexes provokes a strong influence on the chemical shifts of ^1H and ^{13}C , as well as in several complexes with paramagnetic metals, through hyperfine interactions, causing difficult assignation of the conventional NMR spectra [70,71]. In this work, we have focussed our attention on one dimension (1D) assignation of ^1H and ^{13}C spectra for the paramagnetic Cu(II)-Citrulline complex using the Bruker AVANCE III 500 MHz spectrometer and calculations based on

the density functional theory (DFT). In the experimental ^{13}C NMR spectrum in Figure 8a, the first peak is located downfield, assigned as C6A at 161.52 ppm. This signal is assigned to the carbon of the carbonyl moiety of the ureide group. The signals for the C5A/C5B at 57.40/48.83 ppm, C3A/C3B at 38.94/26.99 ppm, and C4A/C4B at 24.78/16.74 ppm were assigned. On the other hand, the ^1H NMR spectrum shows four signals in the upfield region. The first is observed at 1.51 ppm, corresponding to the H4AA/H4BA and H4AB/H4BB pairs of protons. The second signal at 1.87 ppm is assigned for H3AD/H3BD and H3AC/H3BC protons. The third signal at 3.05 ppm corresponds to H5AA/H5BA and H5AB/H5BB protons. The last signal at 3.96 ppm corresponds to a unique H2AA (H_α) proton linked to the Cu(II) atom, suggesting an interaction between the carboxylic and amino groups with the copper ion. A small single peak at 3.25 ppm corresponds to a residual methanol impurity [71,72].

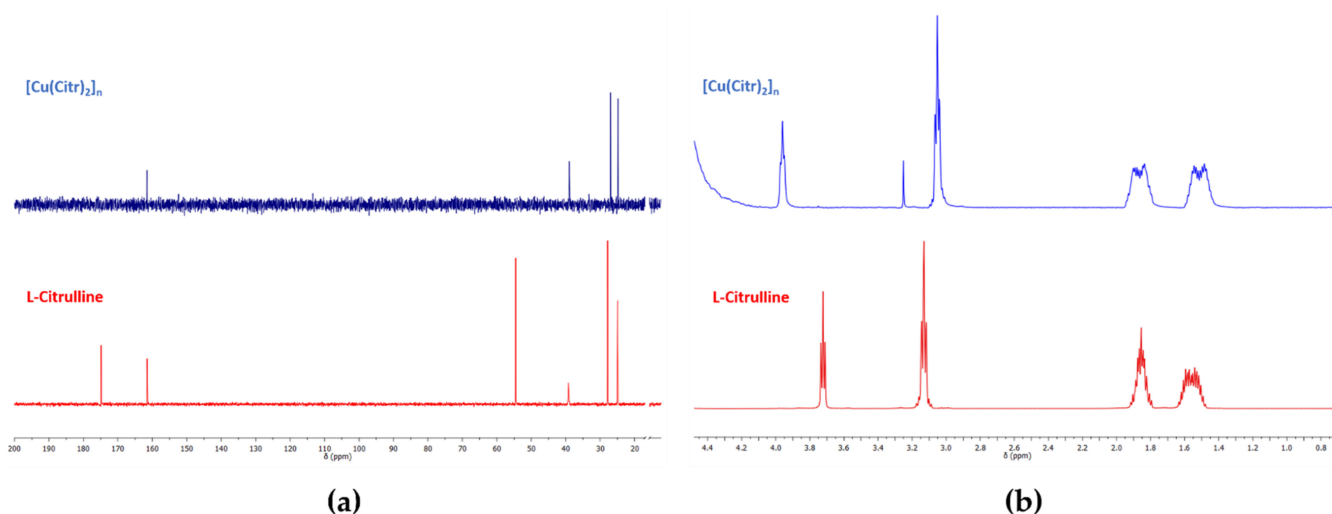


Figure 8. (a) ^{13}C NMR spectrum of $[\text{Cu}(\text{Citr})_2]_n$ in D_2O , and (b) ^1H NMR spectrum of $[\text{Cu}(\text{Citr})_2]_n$ in D_2O .

The theoretical NMR characterization through hyperfine chemical shifts and the effect of the unpaired electron on the Cu(II) on the spin density in the $[\text{Cu}(\text{Citr})_2]_n$ complex was analyzed. The adequate assignment of the ^1H and ^{13}C NMR hyperfine chemical shifts of the complex depends on how the spin density is distributed on the H and C nuclei in the vicinity of Cu(II) with an unpaired electron. The hyperfine shifts are calculated using the UmpW1PW91 functional according to Equations (S1a) and (S1b) shown in the Supplementary Materials Section. Figure 9a shows the labeling of the H and C nuclei for the assignment of the ^{13}C and ^1H NMR chemical shifts, while Figure 9b shows the spin density distribution for one unit of $[\text{Cu}(\text{Citr})_2]_n$. The spin density distribution is mapped in the range of -1.4×10^{-4} u.a. (red color) to 1.4×10^{-4} u.a. (blue color). The Fermi contact shifts (δ_{FC}) are obtained when the spin density values are substituted in Equation (S1a). The total calculated shifts ($\delta_{\text{Total}}^{\text{Calc}}$) are obtained from the Equation (S1b), when the diamagnetic shifts (δ_0) are added to the Fermi contact shifts, which are compared with the experimental chemical shifts (δ_{Exp}). Table 7 shows the assignment of the ^{13}C , and ^1H NMR experimental shifts, δ_{Exp} , the spin density, $\rho_{\alpha\beta}$, the Fermi contact shifts, δ_{FC} , the diamagnetic shifts, δ_0 , the total calculated shifts, $\delta_{\text{Total}}^{\text{Calc}}$ and the ^{13}C and ^1H nuclei assignment in the $[\text{Cu}(\text{Citr})_2]_n$ complex; a good agreement is observed between the experimental and calculated results.

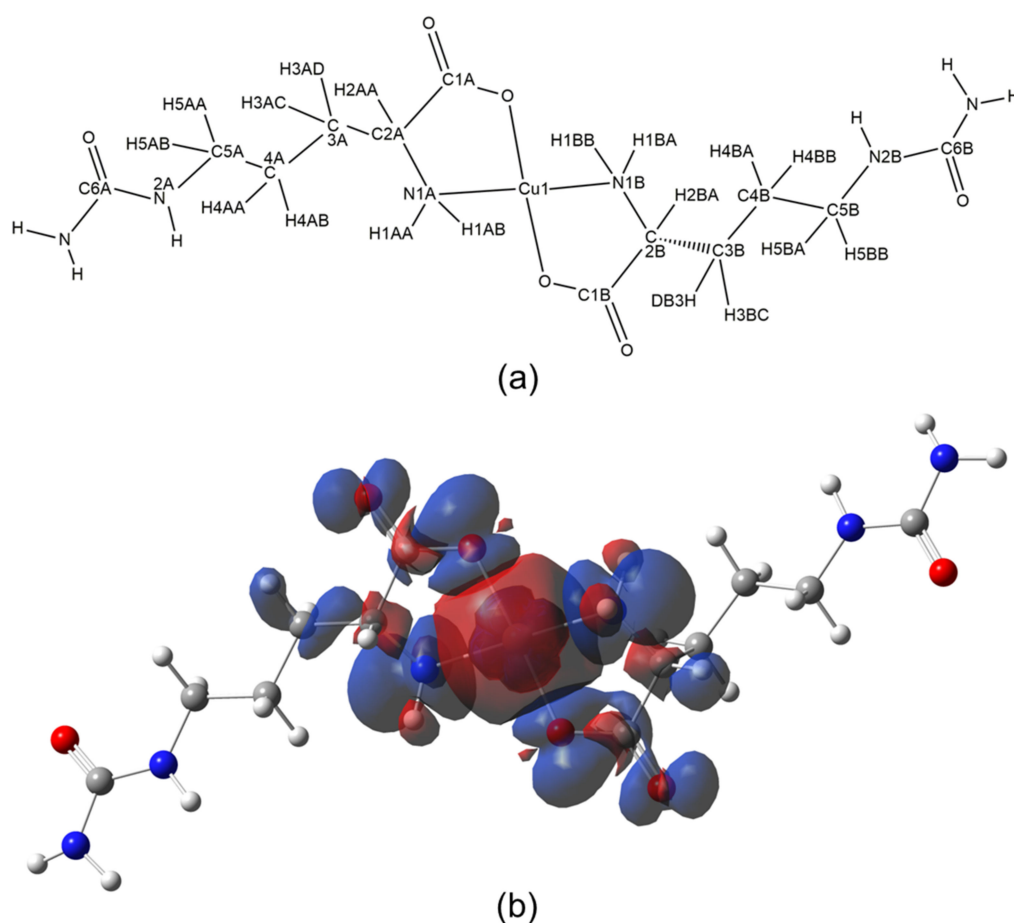


Figure 9. (a) Nomenclature for ^1H and ^{13}C chemical shifts assignment of compound $[\text{Cu}(\text{Citr})_2]_n$, and (b) Spin density of $[\text{Cu}(\text{Citr})_2]_n$ calculated at the level of theory mPW1PW91/6-31G(d)-LANL2DZ and ECP=LANL2DZ.

Table 7. Assignment of the ^{13}C and ^1H experimental and calculated hyperfine chemical shifts of the compound $[\text{Cu}(\text{Citr})_2]_n$ obtained at the level of theory UmPW1PW91/6-31G(d)-LANL2DZ and ECP=LANL2DZ.

Nuclei	δ_{Exp} (ppm)	δ_{FC} (ppm)	δ_0 (ppm)	$\delta_{Total}^{Calc.}$ (ppm)	<Signal Assignment>
^{13}C	161.52	0.00000	0.00	151.32	<C6A>, <C6B>
	57.40, 48.83	0.00014, 0.00005	16.45, 5.88	41.93, 39.54	<C5A>, <C5B>
	38.94, 26.99	0.00004, -0.00005	4.70, -5.88	32.61, 32.39	<C3A>, <C3B>
	24.78, 16.74	-0.00003, -0.00007	3.53, -8.23	27.76, 24.85	<C4A>, <C4B>
	Not observed	-0.00367, -0.00363	-431.23, -426.53	173.05, 176.55	<C1A>, <C1B>
	Not observed	-0.00313, -0.00319	-367.78, -374.83	56.75, 53.63	<C2A>, <C2B>
^1H	3.96	0.00001	1.07	3.32	<H2AA>
	Not observed	0.00101	107.56	3.19	<H2BA>
	3.05	0.00000	0.00	2.91, 3.03	<H5AA>, <H5BA>
	3.05	0.00000	0.00	2.89, 2.89	<H5AB>, <H5BB>
	1.87, 1.87	0.00057, 0.00000	60.70, 0.00	1.85, 1.77	<H3AD>, <H3BD>
	1.87, 1.87	0.00001, 0.00000	1.07, 0.00	1.21, 2.01	<H3AC>, <H3BC>
	1.51	0.00000	0.00	1.33, 1.68	<H4AA>, <H4BA>
	1.51	0.00000	0.00	1.56, 1.57	<H4AB>, <H4BB>
	Not observed	-0.00118, -0.00108	-125.66, -115.02	1.23, 1.68	<H1AA>, <H1BA>
	Not observed	-0.00126, -0.00136	-134.18, -144.83	1.98, 1.87	<H1AB>, <H1BB>

For the ^{13}C NMR, the signal downfield at 151.32 ppm corresponding to C6A is assigned to the carbonyl moiety of the ureide group. The assignment for the C5A/C5B, C3A/C3B, and C4A/C4B are in good agreement with the experimental chemical shifts. The average

difference between values is 1.62 ppm (see Table 7). Two signals are calculated upfield at -311.02 and -321.19 ppm, corresponding to C2A (C_{α}) and C2B ($C_{\alpha'}$) in Figure 8a, respectively, which are not experimentally observed in the range of 10–200 ppm (see Figure 8b). The signals for the C1A and C1B of the carboxylate groups are calculated upfield at -249.97 and -258.17 ppm, respectively. Figure 9b shows the effect of the unpaired electron of the Cu(II) in the distribution of the isosurface of the spin density. It can be observed through the spin density (in blue color) that the complexes with square-plane or octahedral geometries involving the Cu(II) with an unpaired electron, which is in the $d_{x^2-y^2}$ orbital, excluding the Jahn-Teller effect, the atoms close to Cu(II) ion can be affected in their chemical shifts. In addition, the ^{13}C shifts must obey the following relation $\delta_{C_i/C_j} \propto r_{\text{Cu}-C_i}^{-6}$ with the distance Cu–C for the pair of atoms C2A/C2B and C1A/C1B linked to the Cu(II) atom [66]. The values smaller than r^{-6} indicate the displacement of both signals at a very upfield region in the ^{13}C NMR spectrum. From X-ray data in this work, both pairs of carbons are very close to the Cu(II) atom at a distance of 2.74 Å for C2A/C2B and 2.81 Å for C1A/C1B.

Concerning ^1H NMR, as can be observed in Table 6, the chemical shifts obtained from DFT calculations show four signals upfield, which are assigned as follows: the signals at 1.56/1.57 and 1.33/1.68 ppm are assigned to the pairs of protons H4AB/H4BB, and H4AA/H4BA, respectively. The signal at 2.27/2.01 ppm is assigned to the protons H3AC/H3BC. The signal at 1.77 ppm is assigned to H3BD proton, while at 62.55 ppm is assigned to H3AD, which corresponds to the proton affected by the spin density of the unpaired electron of Cu(II) (see Figure 9b). The chemical shifts of 2.89/2.89 and 2.91/3.03 ppm are assigned to the pairs of protons H5AA/H5BA and H5AB/H5BB, respectively. In addition, the theoretical calculations corroborate that a unique signal is observed for the H2AA (H_{α}) proton at 4.83 ppm. In comparison, the signal for the H2BA ($H_{\alpha'}$) is calculated downfield at 110.75 ppm, which is not possible to be experimentally observed. Finally, the DFT calculations suggest that the upfield signals at (-113.34 to -142.96 ppm) can be assigned to the H1AA/H1BA and H1AB/H1BB, and neither are observed at the experimental NMR spectrum.

3.3. Molecular Structure and Non-Covalent Interactions

Figure 10a shows the optimized structure of a triad of copper of the compound $[\text{Cu}(\text{Citr})_2]_n$, and Figure 10b shows the molecular electrostatic potential (MEP). It is also observed that the atom of Cu1 is coordinated with two Citrulline molecules through the two O3A and O3B atoms of carboxylate with distances of Cu–O 1.964–1.980 Å, and two N1A and N1B of amine groups in the equatorial sites with distances of Cu–N 2.018–2.027 Å (Citr1 and Citr2). The two axial positions of the distorted octahedral center are occupied by the O3A and O3B atoms of amide groups of one Citrulline molecule, each one (Citr3 and Citr4) with distances of O–Cu 3.051–3.263 Å. The hydrogen bonds are formed between O2A and O2B atoms of carboxylate with hydrogen atoms H2A/H2B and H3AB/H3BA of amide groups of the adjacent Citrulline. These hydrogen bonds are $\text{NH} \cdots \text{O}$ 1.964–2.101 Å, and $\text{N}-\text{H} \cdots \text{O}$ valence angle of 146.1–153.4°. Figure 10b presents the MEP surface. The electrostatic potential was mapped on the total electronic density with isovalue = 0.004 a.u. in a range of -6.0×10^{-2} (red zones) to 6.0×10^{-2} (blue zones) of electronic density. In addition, the nucleophilic zones (negative charge density) are located on the carboxylate and amide groups of Citrulline. In contrast, the electrophilic zones (deficient density charge) are located on the amine groups and the rest of Citrulline molecules. In addition, yellow and green regions correspond to intermediate electron density zones where the hydrogen bonds are located. These electrophilic and nucleophilic regions are susceptible to interaction with adjacent chains of Citrulline.

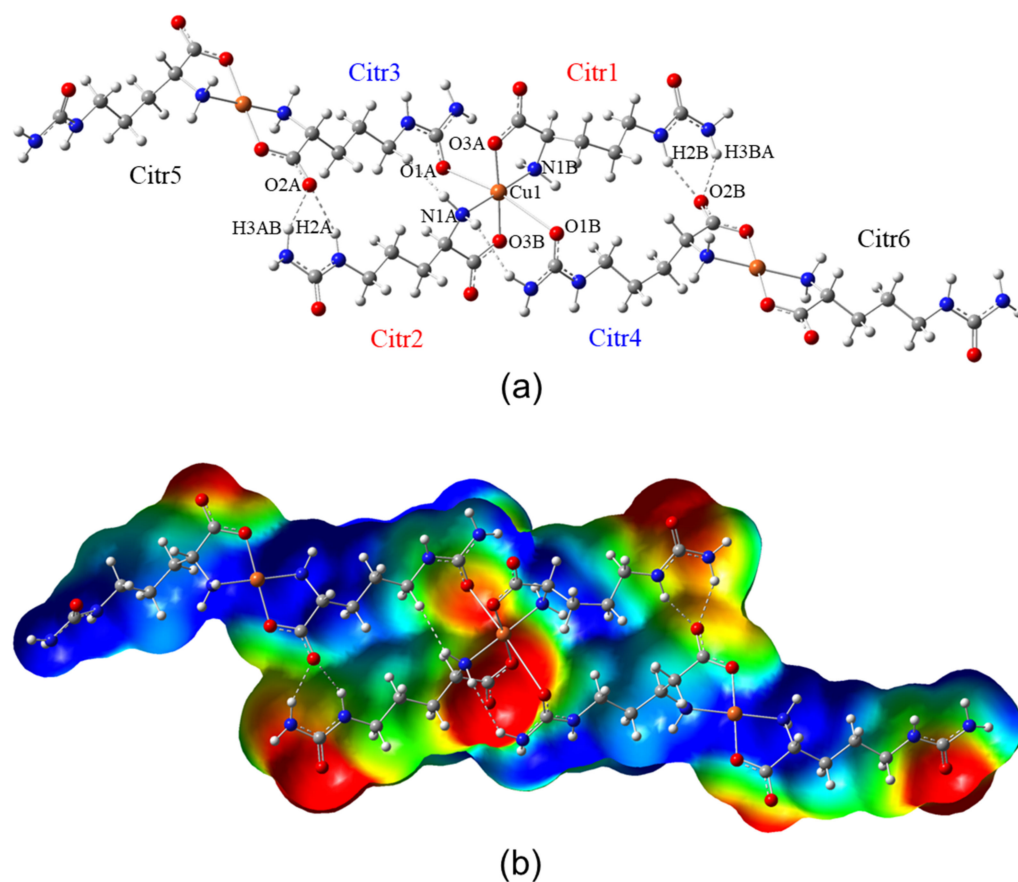


Figure 10. (a) Molecular structure of a representative triad of the compound. (b) Molecular electrostatic potential of compound $[\text{Cu}(\text{Citr})_2]_n$ calculated at the level of theory mPW1PW91/6-31G(d)-LANL2DZ and ECP=LANL2DZ.

The hydrogen bonds were analyzed by electron density, $\rho(r)$, the Laplacian of density, $\nabla^2 \rho(r)$, and the energy of interaction, $E_{\text{H}\dots\text{Y}}$. The results are summarized in Table 8. Figure 11 shows the molecular graphs of compound $[\text{Cu}(\text{Citr})_2]_n$. In this figure, green dots represent bond critical points (BCPs), purple dots represent ring critical points (RCPs), and cyan dots represent cage critical points (CCPs). From the results, it can be seen that the $\rho(r)$ on the BCPs is at the range 0.0172–0.0246 a.u. for the hydrogen bonds N-H \dots O2A and N-H \dots O2B. The calculated interaction energy ($E_{\text{H}\dots\text{Y}}$) is 4.49–6.78 kcal mol $^{-1}$ for these hydrogen bonds connecting Citr1 with Citr4 and Citr2 with Citr3. RCPs with $\rho(r)$ of 0.0080–0.0084 a.u. are observed between the interactions N-H3AB \dots O2A and N-H2A \dots O2A, and N-H2B \dots O2B and N-H3BA \dots O2B, forming stable ring structures of six-atoms.

Table 8. Topological parameters (in a.u.) and interaction energies $E_{\text{H}\dots\text{Y}}$ (in kcal mol $^{-1}$) of compound $[\text{Cu}(\text{Citr})_2]_n$. Atom labels correspond to those shown in Figure 10a.

BCP	$\rho(r)$	$\nabla^2 \rho(r)$	$E_{\text{H}\dots\text{Y}}$
N-H3AB/H3BA \dots O2A/O2B	0.0225–0.0246	0.0760–0.0898	4.52–5.93
N-H2A/H2B \dots O2A/O2B	0.0172–0.0178	0.0770–0.0994	4.49–6.78
Cu1 \dots N1A/N1B	0.0790–0.0807	0.4261–0.4349	39.28–40.47
Cu1 \dots O1A/O1B	0.0749–0.0775	0.5133–0.5334	44.43–57.73
Cu1 \dots O3A/O3B	0.0057–0.0082	0.0156–0.0208	1.26–1.98

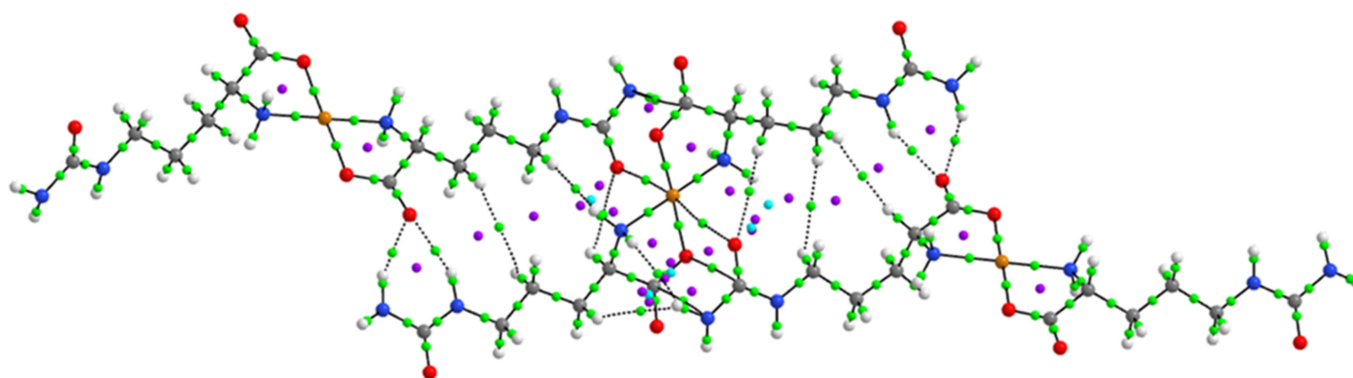


Figure 11. Molecular graphs of compound $[\text{Cu}(\text{Citr})_2]_n$ showing the main BCPs of the H-bonds and RCPs between citrulline molecules.

On the other hand, the BCPs between $\text{Cu1} \cdots \text{N1A}$ and $\text{Cu1} \cdots \text{N1B}$ of the amine group and $\text{Cu1} \cdots \text{O1A}$ and $\text{Cu1} \cdots \text{O1B}$ of the carboxylate group of Citrulline show the highest values of $\rho(r)$ between 0.0749–0.0807 a.u. with $E_{\text{H} \cdots \text{Y}}$ of 39.28–40.47 kcal mol⁻¹ for $\text{Cu1} \cdots \text{N1A/N1B}$ interaction and 44.43–57.73 kcal mol⁻¹ for $\text{Cu1} \cdots \text{O1A/O1B}$ interaction. It indicates the significant metal-ligand non-covalent interactions in the equatorial positions coordinated of the Cu1 atom, similarly to those found for the interactions $\text{Cu} \cdots \text{N}$ of metformin and bipyridine groups at the range of 0.0814–0.1012 a.u., $\text{Cu} \cdots \text{N}$ of imidazol-pyridine and glycine groups at the range of 0.0854–0.0937 a.u. and $\text{Cu} \cdots \text{N}$ of phenanthroline and glutamine groups at the range of 0.0774–0.0864 a.u., in the axial positions of the square pyramidal geometry of Cu in V/Cu heterobimetallic compounds [29,73]. Furthermore, RCPs between $\text{Cu1} \cdots \text{N1A/N1B}$ and $\text{Cu1} \cdots \text{O1A/O1B}$ with $\rho(r)$ of 0.0255–0.0260 a.u. are observed. In addition, several RCPs are observed between the Citrulline chains, indicating the formation of stable rings in the structure. Finally, the BCPs formed between $\text{Cu1} \cdots \text{O3}$ of the amide group of Citrulline at the axial positions of the octahedral geometry have values of $\rho(r)$ between 0.0057–0.0082 a.u. with small interaction energy values of 1.26–1.98 kcal mol⁻¹, indicating that the $\text{Cu1} \cdots \text{O3A}$ and $\text{Cu1} \cdots \text{O3B}$ of the amide group of Citrulline interactions are due to the distorted octahedral geometry.

The Hirshfeld surfaces (HS) and the 2D-fingerprint plot of compound $[\text{Cu}(\text{Citr})_2]_n$ were generated with the function d_{norm} , as shown in Figure 12. Two systems were analyzed: in Figure 12a, the molecules Citr1 and Citr2 are located inside the HS, while Citr3–Citr4 act as ligands outside the HS (see Figure 12a for labeling). In this case, the red spots on the HS are due to the hydrogen bonds between N–H of amide groups inside the HS, acting as a donor, and the oxygen of carboxylate groups of the Citrulline molecules outside the HS, acting as acceptors. In Figure 12b, the molecules Citr3–Citr5 and Citr4–Citr6 are located inside the HS, with Citr1 and Citr2 outside acting as ligands. In this case, the red spots show the same strong hydrogen bond interaction between the oxygen of the carboxylate group inside the HS and the N–H of amide groups outside the HS. In both cases, other red spots are located, indicating the close intermolecular interactions of N–H of amine and carboxylate groups with adjacent Citrulline molecules, and the Cu atom interacting with the oxygen atoms of the amide group coordinated in axial positions of the octahedral geometry. The main hydrogen bonds are indicated with dashed cyan lines in Figure 10. In the 2D-fingerprint plot, the hydrogen bonds $\text{N–H} \cdots \text{O}$ connecting the Citrulline molecules inside and outside the HS have contributions of 17.9% and 21.6%, as shown in Figure 10c. The major contribution to the HS with 45.7% is due to the close intermolecular interactions $\text{H} \cdots \text{H}$ of H of amine and the $-\text{C}_3\text{H}_6$ groups with adjacent Citrulline molecules. Other interactions with minor contributions are $\text{Cu} \cdots \text{O}$ (1.5%), $\text{N} \cdots \text{H}$ (2.4%), and $\text{C} \cdots \text{H}$ (2.0%).

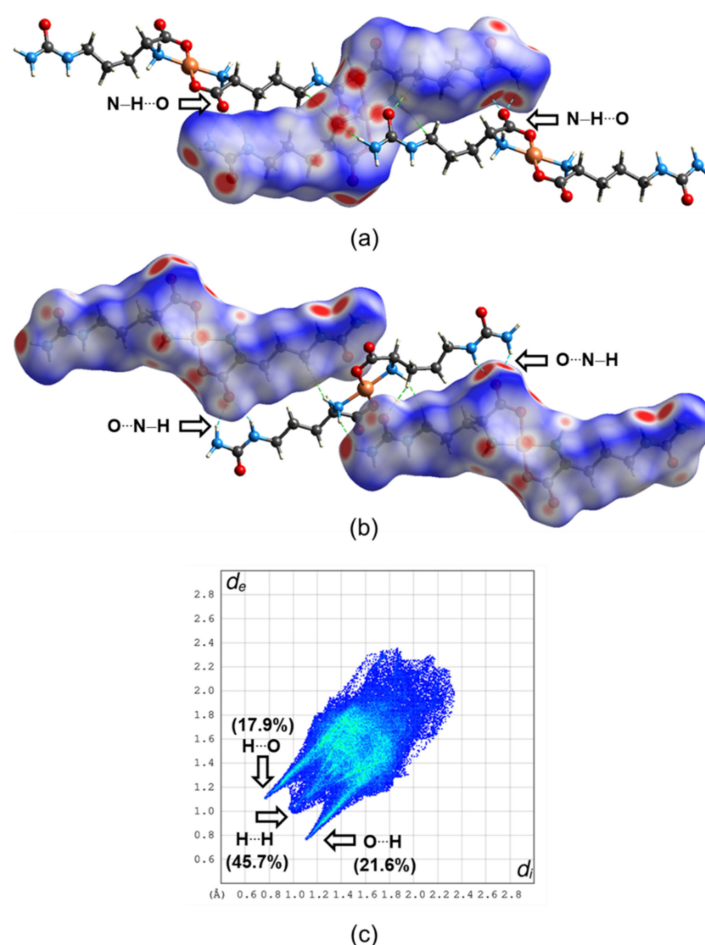


Figure 12. Hirshfeld surfaces mapped with d_{norm} parameter of $[\text{Cu}(\text{Citr})_2]_n$ in two equivalent surfaces: (a) Citr1 and Citr2 inside the HS with Citr3–Citr4 acting as ligands outside the HS, (b) the Citr3–Citr5 and Citr4–Citr6 inside the HS with Citr1 and Citr2 outside the HS, and (c) 2D-fingerprint plot of non-covalent interactions.

4. Discussion

Citrulline is a no-coded amino acid that has received significant attention. The number of papers published on it, from its discovery in 1930 till 2011, is now equal to the ones reported in the last decade.

Citrulline is almost fully present in physiological settings as a zwitterion. Both carboxylic and amine groups can act as Lewis donors at alkaline pH, implying they can complex metallic cations. However, the lateral chain is significantly less complexing as the nitrogen atoms' non-binding electrons are conjugated with a double bond. As a result, Citrulline complexes are identical to those generated by other classical amino acids. However, there is only one crystal structure report in the Cambridge Crystallographic Data-Base. The structure of the palladium complex reported by Mascaliovas et al. [25] was obtained by powder X-ray diffraction, and most studies have been carried out in solution. Although Kurtz proposed the structure of the copper compound in 1939, it was considered an intermediate in the synthesis of Citrulline, and due to its insolubility, it was not characterized thoroughly. However, the work of Ganadu et al., in 1991 [24] on the $[\text{Pd}(\text{Citr})_2]$ gave some light on the structure using spectroscopic methods. The coordination was typical of an aminoacidato, coordinating through the oxygen of the carboxylate and the amino group. No mention of some role of the ureide moiety was presented. Mascaliovas corroborated this, describing the compound as a bis-citrullinate of palladium. The metal is coordinated by two citrulline molecules acting as bidentate ligands in a square planar arrangement with nitrogens and oxygens in *trans* positions. The compound crystallizes on

the *P*-1 space group, so it has an inversion center that requires the presence of the L and D-Citrulline. Interestingly enough, the authors do not mention this fact.

Our findings indicate that Citrulline is a very adaptable chemical, potentially generating several hydrogen-bonding contacts since seven strong interactions were observed in its crystal structure [74]. This is responsible for the polymeric nature of the compound $[\text{Cu}(\text{Citr})_2]_n$, contrary to the case of palladium(II). Palladium prefers square planar geometries; instead, the copper(II) ion could accommodate two monodentate ligands in an axial position in a distorted octahedral environment. Therefore, in this case, the ureide carbonyl group is not-innocent and coordinates the copper(II) ions in the axial positions. The theoretical studies using AIM and Hirshfeld surface analysis also demonstrate that hydrogen bond interactions highly dominate the chemistry of Citrulline. Some complexes based on Cu(II) and amino acids similar to Citrulline have been published. Typically, the synthesis of these compounds uses the L-enantiomer of arginine or ornithine; thus, the complexes obtained contain this enantiomer [75]. In this case, we report a change in the conformation of Citrulline; therefore, due to the coordination of Cu(II), the reactive L-Citrulline is transformed into D-Citrulline. Racemization of amino acids in the presence of metal ions and pyridoxal was discovered by Olivard et al., in 1952 [76]. In this regard, the copper(II) ion was the most effective in the racemization of alanine. Using NMR studies, Abbott and Martell in 1969 showed that aluminum(III) exchange of the α proton of the amino acid in the region pD (pH) 10 [77]. This reaction results in the racemization of the asymmetric center, which is demonstrated by the signals of the racemic complex initially containing one of the amino acid enantiomers.

Recently the term SIST (solubility-induced stereoisomer transformation) was introduced by Fu et al., (2020) [78]. This new concept could be applied to understand $[\text{Cu}(\text{Citr})_2]_n$ since, regardless of the source of L-Citrulline, the final product contains the D stereoisomer. In SIST, one stereoisomer that is below saturation is in rapid equilibrium with the other that is above saturation. A continuous transformation of the more soluble stereoisomer into the less soluble stereoisomer is produced. SIST can theoretically provide double the yield of classical resolutions and does not require the development of stereoselective receptors. It has been a challenge to rapidly racemize free unactivated amino acids because of the weak acidity of the α -carbon-hydrogen atom. Two strong hydrogen bonds can be used in concert to deracemize unactivated amino acids by SIST under mild reaction conditions. The same method can convert readily available L-amino acids into D-amino acids. In addition, if crystallization occurs during a process known as reactive crystallization, it augments the equilibrium reaction yields significantly [79]. Thus, crystallization could propel the development of specific crystals of stereoisomers. Crystallization-induced stereoisomer transformation (CIST) describes a stereoisomer produced by crystallization. In the case of $[\text{Cu}(\text{Citr})_2]_n$, the rapid formation of polymeric chains induces the crystallization of the compound with the D enantiomer imposed by the symmetry of the crystal. It appears that the conjunction of SIST, CIST, hydrogen bonds, and copper allows the rapid formation of catena-trans-syn- $[\text{Cu}(\text{D-Citr})_2]_n$.

The development of effective methods for manufacturing D-amino acids has attracted considerable attention since they are common pharmaceutical building pieces for drugs, such as saxagliptin [80], tadalafil [81], clopidogrel [82], and cyclo-serine [83], against diabetes, erectile dysfunction, heart disease or bacteria. Moreover, D-amino acids are also important in the field of unnatural-peptide-based-therapies, now in growth, such as telaprevir [84], degarelix [85] or carfilzomib [86], antiviral, prostate anticancer, and against multiple myeloma drugs, respectively. Until now, many interesting chemical [87] and biological [88] methods have been developed for making D-amino acids [89]. Therefore, new and interesting findings with this molecule are expected soon.

5. Conclusions

The synthesis and characterization of the bis-citrullinato copper(II) were achieved. Two methodologies and three copper sources were used. Regardless of the method and sources

of copper, the complex $[\text{Cu}(\text{Citr})_2]_n$ was obtained as a pale blue microcrystalline solid. The reaction takes 2 h using hydrothermal synthesis; however, the crystals are extremely small. Using electrosynthesis, which takes 6 to 10 h, bigger crystals were obtained and used for X-ray diffraction studies. Surprisingly, the solid has a polymeric nature, which accounts for its high insolubility. As for the aminoacidato complexes, the amino group's nitrogen and the carboxylic group's oxygen are coordinated to the copper atom. In addition, the carbonyl group of the ureide moiety is not-innocent, and it is coordinated in the axial positions of the copper, which due to a Jahn-Teller effect, has long distances. Therefore, the compound has a copper(II) ion in a distorted octahedral geometry. The aminoacidato ligands are disposed of with oxygen and nitrogen in *trans* positions in the equatorial plane. The stereochemistry of the ligands is D, D, which is contrary to the expected L, L, and the positions of the hydrogens of the α -carbons point in the same direction; thus, the structure corresponds to a syn conformer, although both positions are slightly different.

The molecular structure and non-covalent interactions were analyzed thoroughly and allow us to understand the properties of the compound. The interactions $\text{Cu1} \cdots \text{N1}$ of the amine group and $\text{Cu1} \cdots \text{O2}$ of the carboxylate group of Citrulline showed high interaction energies, indicating the formation of metal-ligand non-covalent interactions in the equatorial positions coordinated by the Cu1 atom. The hydrogen bonds $\text{N-H} \cdots \text{O}$ connecting the Citrulline molecules are clearly characterized in the Hirshfeld surfaces. So, the theoretical studies using AIM and Hirshfeld surface analysis demonstrated that hydrogen bond interactions highly dominate the chemistry of Citrulline. The calculated spectra also were very useful for the assignments of all bands and peaks of the IR, Raman, and ^{13}C and ^1H NMR spectroscopic studies.

As part of our search for Casiopeina[®] analogs, we have synthesized mixed complexes of diimines with lysine, ornithine, glutamine, and asparagine. Currently, attempts are being carried out for Citrulline-mixed complexes since the bis-D-citrullinato is completely insoluble for such purposes. However, the synthesis provides an easy way to obtain the D-Citrulline stereoisomer, which could serve other applications.

Supplementary Materials: The following supporting information can be downloaded at: <https://www.mdpi.com/article/10.3390/cryst12101386/s1>, Equations for NMR calculations. Figure S1: Stereoisomers of Citrulline. Figure S2: Structure of the complex and structure of the zwitter ion of L-Citrulline from CCDC(FIGOQ). Figure S3: Top and side views of the intermediary of the racemization of Citrulline mediated by copper coordination; Figure S4: ORTEP representation of a fragment of the bis-citrullinato Cu(II) polymer. Table S1: Fractional atomic coordinates and isotropic or equivalent isotropic displacement parameters (\AA^2) for (Cu_citrulline); Table S2: Atomic displacement parameters (\AA^2) for (Cu_citrulline); Table S3: Geometric parameters (\AA , $^\circ$) for (Cu_citrulline). Proof of structure deposit and Checkcif.

Author Contributions: D.R.-C. carried out experimental work (synthesis, crystallization, and experimental characterization). FT-Raman measurements were carried out by L.E.S.-d.I.R., F.J.M. and M.E.C. carried out the theoretical characterization. A.G.-G., D.C.-L. and A.R.-D. carried out the X-ray diffraction determination. D.R.-C., E.G.-V., M.E.C., A.G.-G. and B.L.S.-G. wrote and revised the manuscript. D.R.-C. and E.G.-V. conceived and designed this study. All authors contributed extensively to the work presented in this paper. All authors have read and agreed to the published version of the manuscript.

Funding: Projects funded this research: 100108444-VIEP, 100256733-VIEP, and 100233622-VIEP. The PRODEP Academic Group BUAP-CA-263 (SEP, Mexico), and the Ministerio de Universidades and Next Generation for the Margarita Salas contract 401 (Spain).

Data Availability Statement: Data can be obtained directly from authors upon request.

Acknowledgments: Diego Ramírez-Contreras wishes to thank CONACyT (Mexico) M.Sc. fellowship support number 1143792. María Eugenia Castro and Francisco J. Melendez wishes to thank Laboratorio Nacional de Supercomputo del Sureste de México (LNS-BUAP) and the CONACyT network of national laboratories for the computer resources and support provided. Amalia García-García thanks to Ministerio de Universidades and funds Next Generation (Spain).

Conflicts of Interest: The authors declare no conflict of interest.

References

1. Wada, M. On the Occurrence of a New Amino Acid in Watermelon, *Citrullus Vulgaris*, Schrad. *Bull. Agric. Chem. Soc. Jpn.* **1930**, *6*, 32–34. [[CrossRef](#)]
2. Fragkos, K.C.; Forbes, A. Was Citrulline First a Laxative Substance? The Truth about Modern Citrulline and Its Isolation. *Nihon Ishigaku Zasshi* **2011**, *57*, 275–292. [[PubMed](#)]
3. Rimando, A.M.; Perkins-Veazie, P.M. Determination of Citrulline in Watermelon Rind. *J. Chromatogr. A* **2005**, *1078*, 196–200. [[CrossRef](#)] [[PubMed](#)]
4. Kaore, S.N.; Kaore, N.M. Citrulline: Pharmacological Perspectives and Role as a Biomarker in Diseases and Toxicities. In *Biomarkers in Toxicology*; Gupta, R.C., Ed.; Elsevier Inc.: Amsterdam, The Netherlands, 2014; pp. 883–905. ISBN 978-0-12-404630-6.
5. Curis, E.; Crenn, P.; Cynober, L. Citrulline and the Gut. *Curr. Opin. Clin. Nutr. Metab. Care* **2007**, *10*, 620–626. [[CrossRef](#)]
6. Aguayo, E.; Martínez-Sánchez, A.; Fernández-Lobato, B.; Alacid, F. L-Citrulline: A Non-Essential Amino Acid with Important Roles in Human Health. *Appl. Sci.* **2021**, *11*, 3293. [[CrossRef](#)]
7. Curis, E.; Nicolis, I.; Moinard, C.; Osowska, S.; Zerrouk, N.; Bénazeth, S.; Cynober, L. Almost All about Citrulline in Mammals. *Amino Acids* **2005**, *29*, 177–205. [[CrossRef](#)]
8. Papadia, C.; Osowska, S.; Cynober, L.; Forbes, A. Citrulline in Health and Disease. Review on Human Studies. *Clin. Nutr.* **2018**, *37*, 1823–1828. [[CrossRef](#)]
9. Endo, F.; Matsuura, T.; Yanagita, K.; Matsuda, I. Clinical Manifestations of Inborn Errors of the Urea Cycle and Related Metabolic Disorders during Childhood. *J. Nutr.* **2004**, *134*, 1605S–1609S. [[CrossRef](#)]
10. Khalaf, D.; Krüger, M.; Wehland, M.; Infanger, M.; Grimm, D. The Effects of Oral L-Arginine and L-Citrulline Supplementation on Blood Pressure. *Nutrients* **2019**, *11*, 1679. [[CrossRef](#)]
11. Collins, J.K.; Wu, G.; Perkins-Veazie, P.; Spears, K.; Claypool, P.L.; Baker, R.A.; Clevidence, B.A. Watermelon Consumption Increases Plasma Arginine Concentrations in Adults. *Nutrition* **2007**, *23*, 261–266. [[CrossRef](#)]
12. Gramaglia, I.; Velez, J.; Chang, Y.-S.; Caparros-Wanderley, W.; Combes, V.; Grau, G.; Stins, M.F.; van der Heyde, H.C. Citrulline Protects Mice from Experimental Cerebral Malaria by Ameliorating Hypoargininemia, Urea Cycle Changes and Vascular Leak. *PLoS ONE* **2019**, *14*, e0213428. [[CrossRef](#)]
13. Kaore, S.N.; Amane, H.S.; Kaore, N.M. Citrulline: Pharmacological Perspectives and Its Role as an Emerging Biomarker in Future. *Fundam. Clin. Pharmacol.* **2013**, *27*, 35–50. [[CrossRef](#)]
14. Bahri, S.; Zerrouk, N.; Aussel, C.; Moinard, C.; Crenn, P.; Curis, E.; Chaumeil, J.-C.; Cynober, L.; Sfar, S. Citrulline: From Metabolism to Therapeutic Use. *Nutrition* **2013**, *29*, 479–484. [[CrossRef](#)]
15. Rashid, J.; Kumar, S.S.; Job, K.M.; Liu, X.; Fike, C.D.; Sherwin, C.M.T. Therapeutic Potential of Citrulline as an Arginine Supplement: A Clinical Pharmacology Review. *Paediatr. Drugs* **2020**, *22*, 279–293. [[CrossRef](#)]
16. Alghamdi, M.; Alasmari, D.; Assiri, A.; Mattar, E.; Aljaddawi, A.A.; Alattas, S.G.; Redwan, E.M. An Overview of the Intrinsic Role of Citrullination in Autoimmune Disorders. *J. Immunol. Res.* **2019**, *2019*, 7592851. [[CrossRef](#)]
17. Maric, S.; Restin, T.; Muff, J.L.; Camargo, S.M.; Guglielmetti, L.C.; Holland-cunz, S.G.; Crenn, P.; Vuille-dit-bille, R.N. Citrulline, Biomarker of Enterocyte Functional Mass and Dietary Supplement. Metabolism, Transport, and Current Evidence for Clinical Use. *Nutrients* **2021**, *13*, 2794. [[CrossRef](#)]
18. Crans, D.C.; Kostenkova, K. Open Questions on the Biological Roles of First-Row Transition Metals. *Commun. Chem.* **2020**, *3*, 104. [[CrossRef](#)]
19. Fox, S.W. The Preparation of Citrulline by Hydrolysis of Arginine. *J. Biol. Chem.* **1938**, *123*, 687–690. [[CrossRef](#)]
20. Kurtz, A.C. A Simple Synthesis of DL-Citrulline. *J. Biol. Chem.* **1938**, *122*, 477–484. [[CrossRef](#)]
21. Trikha, K.C.; Nair, B.C.; Singh, R.P. Complexation of Bivalent Metal Ions with Amino Acids. I. L-Citrulline Complexes. *Indian J. Chem.* **1968**, *6*, 532.
22. Clarke, E.R.; Martell, A.E. Metal Chelates of Arginine and Related Ligands. *J. Inorg. Nucl. Chem.* **1970**, *32*, 911–926. [[CrossRef](#)]
23. Yamauchi, O.; Sakurai, T.; Nakahara, A. Histidine-Containing Ternary Amino Acid-Copper(II) Complexes. Syntheses and Properties. *J. Am. Chem. Soc.* **1979**, *101*, 4164–4172. [[CrossRef](#)]
24. Ganadu, M.L.; Leoni, V.; Crisponi, G.; Nurchi, V. An Investigation on the Interaction between Palladium(II) and L-Citrulline by ¹H and ¹³C NMR Spectroscopy and Potentiometry. *Polyhedron* **1991**, *10*, 333–336. [[CrossRef](#)]
25. Mascaliavas, B.Z.; Bergamini, F.R.G.; Cuin, A.; Corbi, P.P. Synthesis and Crystal Structure of a Palladium(II) Complex with the Amino Acid L-Citrulline. *Powder Diffr.* **2015**, *30*, 357–361. [[CrossRef](#)]
26. Singh, M.; Shankar, V.; Singh, D.; Krishna, V. Chelation and Stabilization Properties of Citrulline and Uracil with Hg(II) as a Heavy Metal Ion in Solution. *Chem. Sci. Trans.* **2017**, *6*, 646–652. [[CrossRef](#)]
27. Singh, M.; Sinha, S.; Krishna, V. Computed Distribution of Quaternary Complexes of Cu(II), Zn(II) Co(II) and Ni(II) with Citrulline and Tryptophan as Primary Ligand and Thymine as Secondary Ligand. *Proc. Natl. Acad. Sci. India Sect. A—Phys. Sci.* **2021**, *91*, 1–7. [[CrossRef](#)]
28. Martínez-Valencia, B.; Corona-Motolinia, N.D.; Sánchez-Lara, E.; Noriega, L.; Sánchez-Gaytán, B.L.; Castro, M.E.; Meléndez-Bustamante, F.; González-Vergara, E. Cyclo-Tetranadate Bridged Copper Complexes as Potential Double Bullet pro-Metallodrugs for Cancer Treatment. *J. Inorg. Biochem.* **2020**, *208*, 111081. [[CrossRef](#)]

29. Martínez-Valencia, B.; Corona-Motolinia, N.D.; Sánchez-Lara, E.; Sánchez-Gaytán, B.L.; Cerro-López, M.; Mendoza, A.; Castro, M.E.; Meléndez-Bustamante, F.J.; González-Vergara, E. Synthesis and Experimental-Computational Characterization of a Copper/Vanadium Compound with Potential Anticancer Activity. *Crystals* **2020**, *10*, 492. [[CrossRef](#)]
30. Corona-Motolinia, N.D.; Martínez-Valencia, B.; Noriega, L.; Sánchez-Gaytán, B.L.; Mendoza, A.; Meléndez-Bustamante, F.J.; Castro, M.E.; González-Vergara, E. Ternary Copper Complex of L-Glutamine and Phenanthroline as Counterions of Cyclo-Tetranadate Anion: Experimental-Theoretical Characterization and Potential Antineoplastic Activity. *Metals* **2021**, *11*, 1541. [[CrossRef](#)]
31. Su, C.-C.; Tai, T.-Y.; Wu, S.-P.; Wang, S.-L.; Liao, F.-L. Spectroscopic and Electronic Properties of Mixed Ligand Aminoacidatocopper(II) Complexes: Molecular Structure of [Cu(4,7-Dimethyl-1,10-Phenanthroline)(l-Phenylalaninato)](ClO₄). *Polyhedron* **1999**, *18*, 2361–2368. [[CrossRef](#)]
32. Pérez-Benítez, A.; Méndez-Rojas, M.Á.; Bernès, S.; González-Vergara, E. Hybrid (Electrochemical-Chemical) Single Crystal Synthesis of Copper Aspirinate Starting from an Aspirin Tablet: An Undergraduate Bioinorganic Experiment. *Chem. Educ. J.* **2008**, *11*, 11–18.
33. Schotten, C.; Nicholls, T.P.; Bourne, R.A.; Kapur, N.; Nguyen, B.N.; Willans, C.E. Making Electrochemistry Easily Accessible to the Synthetic Chemist. *Green Chem.* **2020**, *22*, 3358–3375. [[CrossRef](#)]
34. Bruker. *APEX3, SAINT, and SADABS*; Bruker AXS Inc.: Madison, WI, USA, 2016.
35. Sheldrick, G.M. SHELXT—Integrated Space-Group and Crystal-Structure Determination. *Acta Crystallogr. Sect. A Found. Adv.* **2015**, *71*, 3–8. [[CrossRef](#)] [[PubMed](#)]
36. Dolomanov, O.V.; Bourhis, L.J.; Gildea, R.J.; Howard, J.A.K.; Puschmann, H. OLEX2: A Complete Structure Solution, Refinement and Analysis Program. *J. Appl. Crystallogr.* **2009**, *42*, 339–341. [[CrossRef](#)]
37. Hohenberg, P.; Kohn, W. Inhomogeneous Electron Gas. *Phys. Rev.* **1964**, *136*, B864–B871. [[CrossRef](#)]
38. Adamo, C.; Jacquemin, D. The Calculations of Excited-State Properties with Time-Dependent Density Functional Theory. *Chem. Soc. Rev.* **2013**, *42*, 845–856. [[CrossRef](#)]
39. Adamo, C.; Barone, V. Exchange Functionals with Improved Long-Range Behavior and Adiabatic Connection Methods without Adjustable Parameters: The MPW and MPW1PW Models. *J. Chem. Phys.* **1998**, *108*, 664–675. [[CrossRef](#)]
40. Rassolov, V.A.; Pople, J.A.; Ratner, M.A.; Windus, T.L. 6-31G * Basis Set for Atoms K through Zn. *J. Chem. Phys.* **1998**, *109*, 1223–1229. [[CrossRef](#)]
41. Hay, P.J.; Wadt, W.R. Ab Initio Effective Core Potentials for Molecular Calculations. Potentials for the Transition Metal Atoms Sc to Hg. *J. Chem. Phys.* **1985**, *82*, 270–283. [[CrossRef](#)]
42. Marenich, A.V.; Cramer, C.J.; Truhlar, D.G. Universal Solvation Model Based on Solute Electron Density and on a Continuum Model of the Solvent Defined by the Bulk Dielectric Constant and Atomic Surface Tensions. *J. Phys. Chem. B* **2009**, *113*, 6378–6396. [[CrossRef](#)]
43. Wolinski, K.; Hinton, J.F.; Pulay, P. Efficient Implementation of the Gauge-Independent Atomic Orbital Method for NMR Chemical Shift Calculations. *J. Am. Chem. Soc.* **1990**, *112*, 8251–8260. [[CrossRef](#)]
44. Frisch, M.J.; Trucks, G.W.; Schlegel, H.B.; Scuseria, G.E.; Robb, M.A.; Cheeseman, J.R. *Gaussian 16, Revision, B.01*; Gaussian Inc.: Pittsburgh, PA, USA, 2016.
45. Dennington, R.D.; Keith, T.A.; Millam, J.M. *Gauss View*; Version 6.0.16; Semichem, Inc.: Shawnee, KS, USA, 2016.
46. Keith, T.A. *TK Gristmill Software*; Version 19.02.13; AIMAll; TK Gristmill Software: Overland Park, KS, USA, 2019.
47. Spackman, P.R.; Turner, M.J.; McKinnon, J.J.; Wolff, S.K.; Grimwood, D.J.; Jayatilaka, D.; Spackman, M.A. CrystalExplorer: A Program for Hirshfeld Surface Analysis, Visualization and Quantitative Analysis of Molecular Crystals. *J. Appl. Crystallogr.* **2021**, *54*, 1006–1011. [[CrossRef](#)]
48. Halcrow, M.A. Interpreting and Controlling the Structures of Six-Coordinate Copper(II) Centres—When Is a Compression Really a Compression? *Dalt. Trans.* **2003**, *23*, 4375–4384. [[CrossRef](#)]
49. Hemissi, H.; Nasri, M.; Abid, S.; Al-Deyab, S.S.; Dhahri, E.; Hlil, E.K.; Rzaigui, M. Crystal Structure, Spectroscopic, Magnetic and Electronic Structure Studies of a Novel Cu(II) Amino Acid Complex [Cu(l-Arg)2(H₂O)]2(P4O12)·8H₂O. *J. Solid State Chem.* **2012**, *196*, 489–497. [[CrossRef](#)]
50. Stevanović, N.; Zlatar, M.; Novaković, I.; Pevec, A.; Radanović, D.; Matić, I.Z.; Đorđić Crnogorac, M.; Stanojković, T.; Vujčić, M.; Gruđen, M.; et al. Cu(II), Mn(II) and Zn(II) Complexes of Hydrazones with a Quaternary Ammonium Moiety: Synthesis, Experimental and Theoretical Characterization and Cytotoxic Activity. *Dalt. Trans.* **2022**, *51*, 185–196. [[CrossRef](#)]
51. Suktanarak, P.; Watchasit, S.; Chitchak, K.; Plainpan, N.; Chainok, K.; Vanalabphatana, P.; Pienpinijtham, P.; Suksai, C.; Tuntulani, T.; Ruangpornvisuti, V.; et al. Tuning the Reactivity of Copper Complexes Supported by Tridentate Ligands Leading to Two-Electron Reduction of Dioxygen. *Dalt. Trans.* **2018**, *47*, 16337–16349. [[CrossRef](#)]
52. Halcrow, M.A. Jahn-Teller Distortions in Transition Metal Compounds, and Their Importance in Functional Molecular and Inorganic Materials. *Chem. Soc. Rev.* **2013**, *42*, 1784–1795. [[CrossRef](#)]
53. Jezowska-Trzebiatowska, B.; Gerega, K.; Vogt, A. Cobalt(II) Complexes Reversibly Uptaking Nitric Oxide in Aqueous Solution. *Inorg. Chim. Acta* **1978**, *31*, 183–185. [[CrossRef](#)]
54. Mofidabadi, A.H.J.; Dehghani, A.; Ramezanzadeh, B. Investigating the Effectiveness of Watermelon Extract-Zinc Ions for Steel Alloy Corrosion Mitigation in Sodium Chloride Solution. *J. Mol. Liq.* **2022**, *346*, 117086. [[CrossRef](#)]

55. Etter, M.C. Encoding and Decoding Hydrogen-Bond Patterns of Organic Compounds. *Acc. Chem. Res.* **1990**, *23*, 120–126. [[CrossRef](#)]
56. Humphrey, W.; Dalke, A.; Schulten, K. VMD: Visual Molecular Dynamics. *J. Mol. Graph.* **1996**, *14*, 33–38. [[CrossRef](#)]
57. Smith, D.W. Ligand Field Splittings in Copper (II) Compounds. In *Structure and Bonding*; Springer: Berlin/Heidelberg, Germany, 1972; Volume 12, pp. 49–112.
58. Hathaway, B.J. A New Look at the Stereochemistry and Electronic Properties of Complexes of the Copper(II) Ion. In *Complex Chemistry. Structure and Bonding*; Springer: Berlin/Heidelberg, Germany, 1984; pp. 55–118. ISBN 978-3-540-13411-4.
59. Stanila, A.; Marcu, A.; Rusu, D.; Rusu, M.; David, L. Spectroscopic Studies of Some Copper(II) Complexes with Amino Acids. *J. Mol. Struct.* **2007**, *834*, 364–368. [[CrossRef](#)]
60. Reddy, S.L.; Endo, T.; Reddy, G.S. Electronic (Absorption) Spectra of 3d Transition Metal Complexes. In *Advanced Aspects of Spectroscopy*; Farrukh, M.A., Ed.; IntechOpen: London, UK, 2012; pp. 3–48.
61. Wojciechowska, A.; Szuster-Ciesielska, A.; Sztandera, M.; Bregier-Jarzębowska, R.; Jarzab, A.; Rojek, T.; Komarnicka, U.K.; Bojarska-Junak, A.; Jezierska, J. L-Argininato Copper(II) Complexes in Solution Exert Significant Selective Anticancer and Antimicrobial Activities. *Appl. Organomet. Chem.* **2020**, *34*, e5698. [[CrossRef](#)]
62. Sciortino, G.; Maréchal, J.-D.; Fábíán, I.; Lihi, N.; Garribba, E. Quantitative Prediction of Electronic Absorption Spectra of Copper(II)-Bioligand Systems: Validation and Applications. *J. Inorg. Biochem.* **2020**, *204*, 110953. [[CrossRef](#)] [[PubMed](#)]
63. Cuevas, A.; Viera, I.; Torre, M.H.; Kremer, E.; Etcheverry, S.B.; Baran, E.J. Infrared Spectra of the Copper (II) Complexes of Amino Acids with Hydrophobic Residues. *Acta Farm. Bonaer.* **1998**, *17*, 213–218.
64. Baran, E.J.; Wagner, C.C.; Torre, M.H.; Kremer, E.; Kögerler, P. Vibrational Spectra of the Cu(II) Complexes of Aspartic and Glutamic Acids. *Acta Farm. Bonaer.* **2000**, *19*, 231–234.
65. Jenkins, A.L.; Larsen, R.A.; Williams, T.B. Characterization of Amino Acids Using Raman Spectroscopy. *Spectrochim. Acta A. Mol. Biomol. Spectrosc.* **2005**, *61*, 1585–1594. [[CrossRef](#)]
66. Nakamoto, K. *Infrared and Raman Spectra of Inorganic and Coordination Compounds: Part B: Applications in Coordination, Organometallic, and Bioinorganic Chemistry*, 6th ed.; John Wiley and Sons: Hoboken, NJ, USA, 2009; ISBN 9780471743392.
67. Sreevalsa, V.G.; Jayalekshmi, S. Investigations on the Growth and Characterization of L-Citrulline Oxalate Monohydrate Single Crystal. *J. Cryst. Growth* **2011**, *324*, 172–176. [[CrossRef](#)]
68. Freire, P.T.C.; Barboza, F.M.; Lima, J.A.; Melo, F.E.A.; Filho, J.M. Raman Spectroscopy of Amino Acid Crystals. In *Raman Spectroscopy and Applications*; Khan, M., Ed.; IntechOpen: London, UK, 2017; pp. 201–223.
69. Fernández, L.E.; Delgado, G.E.; Maturano, L.V.; Tótaró, R.M.; Varetti, E.L. Experimental and Theoretical Vibrational Study of N-Carbamoyl-L-Proline. *J. Mol. Struct.* **2018**, *1168*, 84–91. [[CrossRef](#)]
70. Vusak, D.; Pejic, J.; Jurkovic, M.; Szalontai, G.; Sabolovic, J. Coordination Polymers of Paramagnetic Bis(Leucinato)Copper(II) Diastereomers: Experimental and Computational Study of the Stereoisomerism and Conformations. *CrystEngComm* **2020**, *22*, 5587–5600. [[CrossRef](#)]
71. Mao, J.; Zhang, Y.; Oldfield, E. Nuclear Magnetic Resonance Shifts in Paramagnetic Metalloporphyrins and Metalloproteins. *J. Am. Chem. Soc.* **2002**, *124*, 13911–13920. [[CrossRef](#)]
72. Patil, B.H.; Peraje, P.; Naik, D.; Rajaramkrishna, R.; Dittmer, J.; Kumar, S.; Swamy, K. Experimental ¹H and ¹³C Solid-State NMR Signal Assignment of Paramagnetic Copper (II) 2-Pyrazine-Carboxylate Complex Using Density Functional Theory Calculations. *J. Phys. Conf. Ser.* **2021**, *1819*, 012032. [[CrossRef](#)]
73. Corona-Motolinia, N.D.; Martínez-Valencia, B.; Noriega, L.; Sánchez-Gaytán, B.L.; Méndez-Rojas, M.Á.; Melendez, F.J.; Castro, M.E.; González-Vergara, E. Synthesis, Crystal Structure, and Computational Methods of Vanadium and Copper Compounds as Potential Drugs for Cancer Treatment. *Molecules* **2020**, *25*, 4679. [[CrossRef](#)]
74. Caruso, A.; Rossi, M.; Gahn, C.; Caruso, F. A Structural and Computational Study of Citrulline in Biochemical Reactions. *Struct. Chem.* **2017**, *28*, 1581–1589. [[CrossRef](#)]
75. Jia, G.-G.; Liu, Y.; Zheng, Y.-G.; Zhang, L.; Liu, L.; Ling, X.; Gou, L.-S.; Yin, C.; Zhuang, X.-M. A Novel Preparation of L-Citrulline and L-Homocitrulline. *J. Chem. Soc. Pak.* **2012**, *34*, 451–454.
76. Olivard, J.; Metzler, D.E.; Snell, E.E. Catalytic Racemization of Amino Acids by Pyridoxal and Metal Salts. *J. Biol. Chem.* **1952**, *199*, 669–674. [[CrossRef](#)]
77. Abbott, E.H.; Martell, A.E. Mechanism of Formation, Structure, Stereochemistry, and Racemization of Bis[Pyridoxylidene (Amino Acidato)]Aluminum(III) Complexes. *J. Am. Chem. Soc.* **1970**, *92*, 5845–5851. [[CrossRef](#)]
78. Fu, R.; So, S.M.; Lough, A.J.; Chin, J. Hydrogen Bond Assisted L to D Conversion of α -Amino Acids. *Angew. Chemie Int. Ed.* **2020**, *59*, 4335–4339. [[CrossRef](#)]
79. Kolarović, A.; Jakubec, P. State of the Art in Crystallization-Induced Diastereomer Transformations. *Adv. Synth. Catal.* **2021**, *363*, 4110–4158. [[CrossRef](#)]
80. Augeri, D.J.; Robl, J.A.; Betebenner, D.A.; Magnin, D.R.; Khanna, A.; Robertson, J.G.; Wang, A.; Simpkins, L.M.; Taunk, P.; Huang, Q.; et al. Discovery and Preclinical Profile of Saxagliptin (BMS-477118): A Highly Potent, Long-Acting, Orally Active Dipeptidyl Peptidase IV Inhibitor for the Treatment of Type 2 Diabetes. *J. Med. Chem.* **2005**, *48*, 5025–5037. [[CrossRef](#)]
81. Daugan, A.; Grondin, P.; Ruault, C.; Le Monnier De Gouville, A.C.; Coste, H.; Kirilovsky, J.; Hyafil, F.; Labaudinière, R. The Discovery of Tadalafil: A Novel and Highly Selective PDE5 Inhibitor. 1: 5,6,11,11a-Tetrahydro-1H-Imidazo[1',5':1,6]Pyrido[3,4-b]Indole-1,3(2H)-Dione Analogues. *J. Med. Chem.* **2003**, *46*, 4525–4532. [[CrossRef](#)]

82. Herbert, J.M.; Frehel, D.; Vallee, E.; Kieffer, G.; Gouy, D.; Berger, Y.; Necciari, J.; Defreyn, G.; Maffrand, J.P. Clopidogrel, A Novel Antiplatelet and Antithrombotic Agent. *Cardiovasc. Drug Rev.* **1993**, *11*, 180–198. [[CrossRef](#)]
83. Kuehl, F.A.; Wolf, F.J.; Trenner, N.R.; Peck, R.L.; Howe, E.; Hunnewell, B.D.; Downing, G.; Newstead, E.; Folkers, K.; Buhs, R.P.; et al. D-4-Amino-3-Isoxazolidone, A New Antibiotic. *J. Am. Chem. Soc.* **1955**, *77*, 2344–2345. [[CrossRef](#)]
84. Kwong, A.D.; Kauffman, R.S.; Hurter, P.; Mueller, P. Discovery and Development of Telaprevir: An NS3-4A Protease Inhibitor for Treating Genotype 1 Chronic Hepatitis C Virus. *Nat. Biotechnol.* **2011**, *29*, 993–1003. [[CrossRef](#)]
85. Anderson, J. Degarelix: A Novel Gonadotropin-Releasing Hormone Blocker for the Treatment of Prostate Cancer. *Futur. Oncol.* **2009**, *5*, 433–443. [[CrossRef](#)]
86. Khan, M.L.; Stewart, A.K. Carfilzomib: A Novel Second-Generation Proteasome Inhibitor. *Futur. Oncol.* **2011**, *7*, 607–612. [[CrossRef](#)]
87. So, S.M.; Kim, H.; Mui, L.; Chin, J. Mimicking Nature to Make Unnatural Amino Acids and Chiral Diamines. *Eur. J. Org. Chem.* **2012**, *2012*, 229–241. [[CrossRef](#)]
88. Breuer, M.; Ditrich, K.; Habicher, T.; Hauer, B.; Keßeler, M.; Stürmer, R.; Zelinski, T. Industrial Methods for the Production of Optically Active Intermediates. *Angew. Chem. Int. Ed. Engl.* **2004**, *43*, 788–824. [[CrossRef](#)]
89. Blaskovich, M.A.T. Unusual Amino Acids in Medicinal Chemistry. *J. Med. Chem.* **2016**, *59*, 10807–10836. [[CrossRef](#)]